Final Progress Report for Research Projects Funded by Health Research Grants

Instructions: Please complete all of the items as instructed. Do not delete instructions. Do not leave any items blank; responses must be provided for all items. If your response to an item is "None", please specify "None" as your response. "Not applicable" is not an acceptable response for any of the items. There is no limit to the length of your response to any question. Responses should be single-spaced, no smaller than 12-point type. The report **must be completed using MS Word**. Submitted reports must be Word documents; they should not be converted to pdf format. Questions? Contact Health Research Program staff at 717-231-2825.

1. **Grantee Institution:** Trustees of the University of Pennsylvania

2. **Reporting Period (start and end date of grant award period):** 1/1/2011 – 12/31/2014

3. **Grant Contact Person (First Name, M.I., Last Name, Degrees):** Gearline Robinson-Hall, BSF

4. **Grant Contact Person's Telephone Number:** 215-746-6821

5. **Grant SAP Number:** 4100054874

6. **Project Number and Title of Research Project:** 3-Control of Somatic Stem Cell Potency and Tumorigenesis by Musashi RNA Binding

7. **Start and End Date of Research Project:** 1/1/2011 – 6/30/2014

8. **Name of Principal Investigator for the Research Project:** Christopher J. Lengner, PhD

9. **Research Project Expenses**.

   9(A) Please provide the total amount of health research grant funds spent on this project for the entire duration of the grant, including indirect costs and any interest earned that was spent:

   $ 923,616

   9(B) Provide the last names (include first initial if multiple individuals with the same last name are listed) of **all** persons who worked on this research project and were supported with health research funds. Include position titles (Principal Investigator, Graduate Assistant, Post-doctoral Fellow, etc.), percent of effort on project and total health research funds expended for the position. For multiple year projects, if percent of effort varied from year to year, report in the % of Effort column the effort by year 1, 2, 3, etc. of the project (x% Yr 1; z% Yr 2-3).

Last Name, First Name	Position Title	% of Effort on Project	Cost
Yu, Zhengquan	Postdoctoral Fellow	Yr 1 – 69%; Yr 2 – 55%	50,664.79
Leu, Nicolae	Research Specialist	Yr 1 – 2%; Yr 2 -1%	18,435.68
Cedeno, Ryan	Graduate Student	100%	44,791.73
Wang, Shan	Graduate Student/Visiting Scholar	100	11,666.74
Ddamba, Angela	Research Associate	50%	5,000.00
Parada, Kimberly	Research Associate	Yr1 – 100%; Yr 2 – 50%	34,615.85
Lengner, Christopher	Co-Investigator	30	14,680.13
Woo, Dong-Hun	Postdoctoral Fellow	100	22,170
Shankar, Sheila	Undergraduate Student	100	2,2645.00
Gentilella, Antonio	Postdoctoral Fellow	100	6,864.08

9(C) Provide the names of **all** persons who worked on this research project, but who *were not* supported with health research funds. Include position titles (Research Assistant, Administrative Assistant, etc.) and percent of effort on project. For multiple year projects, if percent of effort varied from year to year, report in the % of Effort column the effort by year 1, 2, 3, etc. of the project (x% Yr 1; z% Yr 2-3).

Last Name, First Name	Position Title	% of Effort on Project
Yousefi, Maryam	Graduate Student	50
Li, Ning	Postdoctoral Fellow	50

9(D) Provide a list of **all** scientific equipment purchased as part of this research grant, a short description of the value (benefit) derived by the institution from this equipment, and the cost of the equipment.

Type of Scientific Equipment	Value Derived	Cost
None		

10. Co-funding of Research Project during Health Research Grant Award Period. Did this research project receive funding from any other source during the project period when it was supported by the health research grant?

Yes___X__ No_____

If yes, please indicate the source and amount of other funds:

Abramson Cancer Center American Cancer Society IRG-78-002-32
Lengner (PI) Control of Stem cell-driven intestinal tumorigenesis by Musashi RNA binding proteins 02/01/2011-12/31/2011 - $30,000

W.W. Smith Charitable Trust Cancer Fellowship Control of stem cell-driven tumorigenesis Lengner (PI) 01/01/2012-12/31/2012 - $100,000

Penn Center for Molecular Studies in Digestive and Liver Diseases Pilot Program
Lengner (PI) Control of Stem cell-driven intestinal tumorigenesis by Musashi RNA binding proteins 07/01/2011-06/30/2013 - $50,000

11. Leveraging of Additional Funds

11(A) As a result of the health research funds provided for this research project, were you able to apply for and/or obtain funding from other sources to continue or expand the research?

Yes___X___ No_____

If yes, please list the applications submitted (column A), the funding agency (National Institutes of Health—NIH, or other source in column B), the month and year when the application was submitted (column C), and the amount of funds requested (column D). If you have received a notice that the grant will be funded, please indicate the amount of funds to be awarded (column E). If the grant was not funded, insert "not funded" in column E.

Do not include funding from your own institution or from CURE (tobacco settlement funds). Do not include grants submitted prior to the start date of the grant as shown in Question 2. If you list grants submitted within 1-6 months of the start date of this grant, add a statement below the table indicating how the data/results from this project were used to secure that grant.

A. Title of research project on grant application	B. Funding agency (check those that apply)	C. Month and Year Submitted	D. Amount of funds requested:	E. Amount of funds awarded:
Deregulation of MSI RNA-binding proteins promotes intestinal tumorigenesis	XNIH ☐ Other federal (specify:_____) ☐ Nonfederal source (specify:_)	6/2012	$1,250,000	$975,250
Control of gastrointestinal radiosensitivity by an Msi-mTorc1 signaling axis	XNIH ☐ Other federal (specify:_____) ☐ Nonfederal source (specify:_)	10/2014	$1,250,000	Not funded (yet)

11(B) Are you planning to apply for additional funding in the future to continue or expand the research?

Yes_____X____ No_____

If yes, please describe your plans:

The work initiated by this project has led to a shift in the dogma of how we believe colon cancer is initiated. The findings of this proposal clearly demonstrated the oncogenic functions of Msi proteins in both mouse and human systems. The unexpected finding from this work was that Msi acts specifically on a rare, dormant intestinal stem cell that has been underappreciated in the literature, which has historically been focused on the highly proliferative, active stem cell as the driver of intestinal cancers. We are now focusing on the role of this dormant stem cell not only as a driver of colorectal cancer, but also in control of normal intestinal regeneration after injury such as ischemia-reperfusion, high-dose gamma irradiation, etc. The role of Msi and the dormant intestinal stem cell in regeneration after injury was the central focus of a recently submitted R01 at the NIDDK. This grant scored well, receiving favorable reviews, and while it may not get funded on the initial submission (A0) is certainly a strong candidate for funding on the resubmission (A1).

12. Future of Research Project. What are the future plans for this research project?

The work initiated by this HRFF award has led to a shift in the dogma of how we believe colon cancer is initiated. The findings of this proposal clearly demonstrated the oncogenic functions of Msi proteins in both mouse and human systems. The unexpected finding from this work was that Msi acts specifically on a rare, dormant intestinal stem cell that has been underappreciated in the literature, which has historically been focused on the highly proliferative, active stem cell as the driver of intestinal cancers. We are now focusing on the role of this dormant stem cell not only as a driver of colorectal cancer, but also in control of normal intestinal regeneration after injury such as ischemia-reperfusion, high-dose gamma irradiation, etc. The role of Msi and the dormant intestinal stem cell in regeneration after injury was the central focus of a recently submitted R01 at the NIDDK. This grant scored well, receiving favorable reviews, and while it may not get funded on the initial submission (A0) is certainly a strong candidate for funding on the resubmission (A1).

13. New Investigator Training and Development. Did students participate in project supported internships or graduate or post-graduate training for at least one semester or one summer?

Yes___X___ No_____

If yes, how many students? Please specify in the tables below:

	Undergraduate	Masters	Pre-doc	Post-doc
Male			1	4
Female	1		2	
Unknown				
Total	**1**		**3**	**4**

	Undergraduate	Masters	Pre-doc	Post-doc
Hispanic			1	
Non-Hispanic	1		2	4
Unknown				
Total	**1**		**3**	**4**

	Undergraduate	Masters	Pre-doc	Post-doc
White				1
Black				
Asian			1	3
Other	1		2	
Unknown				
Total	**1**		**3**	**4**

14. **Recruitment of Out-of–State Researchers**. Did you bring researchers into Pennsylvania to carry out this research project?

    Yes___X_____ No_____

    If yes, please list the name and degree of each researcher and his/her previous affiliation:

    Shan Wang, Graduate Student (receiving Ph.D. in 2015 based on work done on this project), Beijing Agricultural University, Beijing, China

15. **Impact on Research Capacity and Quality**. Did the health research project enhance the quality and/or capacity of research at your institution?

    Yes__X_____ No_____

    If yes, describe how improvements in infrastructure, the addition of new investigators, and other resources have led to more and better research.

    This project enabled the hiring of researchers that have improved the standing of the University of Pennsylvania Graduate School of Biomedical Sciences. Particularly, a foreign Ph.D. student from Iran, Maryam Yousefi, was awarded a very prestigious Howard Hughes fellowship for a proposal stemming from this award. Another Ph.D. student, Ryan Cedeno, is a Hispanic minority who has contributed to this work and has received federal funding. A postdoctoral fellow, Zhengquan Yu, recently started his own lab and faculty position at the China Agricultural University in Beijing. Another postdoctoral fellow, Ning Li, recently was awarded a green card for his extraordinary scientific contributions and we hope to retain him at the University of Pennsylvania. Thus, this award has enriched the academic environment not only here at Penn, but has also had global impact, both directly and indirectly.

16. Collaboration, business and community involvement.

16(A) Did the health research funds lead to collaboration with research partners outside of your institution (e.g., entire university, entire hospital system)?

Yes__X___ No_____

If yes, please describe the collaborations:

This work on Msi oncoproteins in colon cancer has led to the initiation of ongoing collaborations with researchers now using our models to study these proteins in the skin (University of Colorado) and in lung cancer (Fox Chase Cancer Center).

16(B) Did the research project result in commercial development of any research products?

Yes_____ No___X___

If yes, please describe commercial development activities that resulted from the research project:

16(C) Did the research lead to new involvement with the community?

Yes_____ No___X__

If yes, please describe involvement with community groups that resulted from the research project:

17. Progress in Achieving Research Goals, Objectives and Aims.

List the project goals, objectives and specific aims (as contained in the grant agreement). Summarize the progress made in achieving these goals, objectives and aims for the period that the project was funded (i.e., from project start date through end date). Indicate whether or not each goal/objective/aim was achieved; if something was not achieved, note the reasons why. Describe the methods used. If changes were made to the research goals/objectives/aims, methods, design or timeline since the original grant application was submitted, please describe the changes. Provide detailed results of the project. Include evidence of the data that was generated and analyzed, and provide tables, graphs, and figures of the data. List published abstracts, poster presentations and scientific meeting presentations at the end of the summary of progress; peer-reviewed publications should be listed under item 20.

This response should be a DETAILED report of the methods and findings. It is not sufficient to state that the work was completed. Insufficient information may result in an unfavorable

performance review, which may jeopardize future funding. If research findings are pending publication you must still include enough detail for the expert peer reviewers to evaluate the progress during the course of the project.

Health research grants funded under the Tobacco Settlement Act will be evaluated via a performance review by an expert panel of researchers and clinicians who will assess project work using this Final Progress Report, all project Annual Reports and the project's strategic plan. After the final performance review of each project is complete, approximately 12-16 months after the end of the grant, this Final Progress Report, as well as the Final Performance Review Report containing the comments of the expert review panel, and the grantee's written response to the Final Performance Review Report, will be posted on the CURE Web site.

There is no limit to the length of your response. Responses must be single-spaced below, no smaller than 12-point type. If you cut and paste text from a publication, be sure symbols print properly, e.g., the Greek symbol for alpha (α) and beta (ß) should not print as boxes (□) and include the appropriate citation(s). DO NOT DELETE THESE INSTRUCTIONS.

Project Overview

The drosophila RNA binding protein musashi and its mammalian orthologs Msi1 and Msi2 have been shown to govern asymmetric cell division as well as stem cell potency and tumorigenesis in the hematopoietic system, potentially providing a common link between these three processes. In the intestine, Msi proteins are expressed in putative stem cell compartments where asymmetric cell division is observed in homeostatic tissue. Activating mutations in the Wnt signaling pathway initiate the progression of colorectal cancer and abrogate the observed asymmetric mitoses. Here we propose to determine the functional contribution of Msi proteins to the onset and progression of colorectal cancer. Both gain and loss of function approaches for Msi1 and Msi2 will be used in a murine model of colorectal cancer driven by activating Wnt mutations in intestinal stem cells. Drug-inducible ectopic Msi1 and Msi2 expression in the intestine will determine the oncogenic capacity of Msi proteins, and conditional deletion of Msi1 and Msi2 both broadly and in tumor-initiating stem cells at the onset and during the progression of colorectal cancer will precisely determine the contribution of these genes in this stem cell-driven disease. Our findings will provide novel and valuable insight into the mechanisms by which regulators of asymmetric cell division impact both epithelial stem cell function and oncogenic transformation and will provide a foundation for determining the clinical value of Msi proteins as diagnostic markers and therapeutic targets.

Summary of progress on Specific Aims.

Specific Aims:
Aim 1 - Identification of Msi-expressing cells in APC^{min}-driven cancer
-We have successfully completed Aim1 and identified cells expressing Msi1 and Msi2 both in cancers arising in the APC^{min} model of intestinal cancer, as well as in human intestinal cancers using both immunohistochemistry detecting Msi proteins and gene expression analysis on larger cohorts of patient tumors and age-matched (or adjacent normal) control tissues. Below we

summarize the findings as they relate to Msi1. Findings related to Msi2 are in press at *Nature Communications* and will be published in March of 2015 (*Wang and Li et al., Nat. Comm. 2015*).

Aim 2 - Determining potential oncogenicity of Msi proteins in the intestine
-We have successfully completed Aim 2 and demonstrated that both Msi1 and Msi2 act as intestinal oncogenes in both murine and human systems. We have further elucidated the molecular mechanisms through which these oncoproteins act in detail, also in both murine and human systems. The data for Msi1 are detailed below and the data for Msi2 are contained in the attached *Nature Communications* publication.

Aim 3 - Effects of Msi inactivation during *APC^{min}*-driven tumorigenesis
-We have successfully completed Aim 3 and demonstrated that Msi1 and Msi2 function redundantly to promote tumorigenesis in the APC^{min} model of intestinal cancer such that inactivation of Msi1 or Msi2 alone is insufficient to abrogate tumor formation, but inactivation of both Msi proteins abrogates tumor formation. These data are described in detail below. We have further extended this analysis to an inflammation driven model of colorectal cancer (AOM-DSS) and similarly found an absolute requirement for Msi activity in this model (data not shown). We further extended the study of Msi loss of function on tumor cell growth to human colorectal cancer cell lines *in vitro* and using xenograft assays and found that in some lines that express only MSI2, inhibition of MSI2 only was sufficient to abrogate tumor growth, whereas in cell lines coexpressing both MSI1 and MSI2, both MSI family members needed to be inhibited to abrogate tumor growth. The data for MSI1 and MSI2 combinatorial inhibition are presented below, and the data for MSI2 inhibition only is contained in the d *Nature Communications* publication listed in Question 20.

Taken together, we have successfully completed all of the outlined Specific Aims for this award. Below is a detailed account of our results.

Msi1 is Expressed in Human Cancers of the Gastrointestinal Tract and in Early Adenomas Resulting from APC Loss.
We initially sought to verify reports of MSI1 expression in human gastrointestinal (GI) cancers (Levin et al., 2010; Li et al., 2011; Liu et al., 2002; Wang et al., 2011). Examination of transcriptome profiles of several types of primary GI tumors revealed that *MSI1* expression is elevated in nearly all of these malignancies, and immunohistochemistry of CRC samples shows strong MSI1 expression in all grades of adenocarcinoma (Figure 1A, B). While MSI1 functions as a cytoplasmic RNA binding protein, we increasingly observed MSI1-positive nuclei in high-grade adenocarcinomas, including mucinous adenocarcinomas, however the significance of this localization is unclear (Figure 1B and not shown). We also examined Msi1 expression in early adenomas resulting from APC loss in the *APC$^{min/+}$* model of intestinal transformation, previously reported to express Msi1 (Potten et al., 2003). *APC$^{min/+}$* mice harbor a germline inactivating mutation (C-terminal truncation) in one *APC* allele. Adult mice spontaneously undergo loss of heterozygosity (LOH) at the remaining wildtype allele, triggering stochastic adenoma formation when LOH occurs in intestinal stem cells (Barker et al., 2009). In adenomas resulting from *APC* LOH, Msi1 protein was detected throughout the tumor cell cytoplasm along with cytoplasmic and nuclear accumulation of β-catenin (Figure 1C).

In mice *APC* inactivation results in tumor formation only when it occurs in intestinal stem cells (Barker et al., 2009). We therefore examined Msi1 distribution in the intestinal stem cell compartment. Msi1 protein colocalized in crypt base columnar stem cells with Lgr5 expression marked by an *Lgr5-eGFP-IRES-CreER* allele (Barker et al., 2007). Further, the Msi1 expression domain extended beyond Lgr5-positive CBCs into the +4 position where reserve intestinal stem cells reside (He et al., 2007; Montgomery et al.; Sangiorgi and Capecchi, 2008; Takeda et al., 2011) (Figure 1D). Thus, Msi1 is expressed in stem cells of the intestinal crypt and its aberrant activation is an early event in the ontogeny of intestinal adenoma formation.

Oncogenic MSI/Msi Activity is Required for Intestinal Tumorigenesis.

Given the expression of MSI1 in human intestinal cancers and of Msi1 in adenomas arising in $APC^{min/+}$ mice, we sought to determine whether MSI1/Msi1 plays a major oncogenic role in these settings through loss-of-function studies. We first knocked down MSI1 in a panel of human colorectal cancer cells (including RKO, SW48, HCT116, and LoVo) and monitored their proliferative capacity. Knockdown of MSI1 alone had inhibitory to insignificant effects on proliferation of these cells, depending on the cell line (Figure 2A, B and S1A, B). Msi1 is highly homologous to and frequently co-expressed with the second mammalian Msi family member Msi2 in numerous tissues, and they are known to function redundantly in neural progenitor cells (Sakakibara et al., 2002). We therefore assessed tumor cell growth upon knockdown of both MSI family members. In this context there was significant abrogation of tumor cell growth *in vitro* (Figure 2A and S6) indicating that MSI proteins act redundantly to promote CRC growth. Comparison of MSI1/2 knockdown with knockdown of β-CATENIN indicates that MSI1/2 inhibition was as potent as β-CATENIN inhibition in blocking growth. Further, murine xenograft assays in RKO and HCT116 cells revealed similar effects of inhibition of MSI1/2 or β-CATENIN in abrogating tumor growth *in vivo* (Figure 2C, D and S1C, D), and combinatorial knockdown of MSI1/2 and β-CATENIN synergistically inhibited tumorigenesis, resulting complete absence of tumor formation (Figure 2C, D). Interestingly, knockdown of β-CATENIN had no discernable effect on MSI1 protein levels, and knockdown of MSI proteins had little to no effect on transcriptionally active (nuclear) β-CATENIN levels in these cells (Figure 2B), suggesting that MSI and β-CATENIN act in parallel pathways to promote CRC growth.

Ultimately, we sought to determine if Msi activity was required for tumor initiation and progression upon APC loss in the $APC^{min/+}$ model of intestinal tumorigenesis. We therefore generated conditional loss of function alleles for both *Msi1* and *Msi2* and crossed them into an $APC^{min/+}$ background (Figure 2E and S1E, F). As expected from our human CRC data, ablation of *Msi1* alone using a Villin-CreER transgene (el Marjou et al., 2004) was insufficient to significantly abrogate tumor formation (data not shown). Ablation of both *Msi1* and *Msi2*, however, resulted in a significant decrease in tumor burden in $APC^{min/+}$*::Msi1*$^{flx/flx}$*::Msi2*$^{flx/flx}$*::Villin-CreER* mice (Figure 2E, F). We were surprised to find that some tumors did form in these mice, even after multiple doses of Tamoxifen and high recombination efficiency determined by Southern blotting. We therefore stained the residual tumors found in $APC^{min/+}$*::Msi1*$^{flx/flx}$*:: Msi2*$^{flx/flx}$*::Villin-CreER* mice and observed that 100% (68/68) of these tumors were immunoreactive for Msi1, Msi2, or both Msi1 and Msi2 in the same tumor, indicating that one or more *Msi* alleles escaped recombination in those clones (Figure 2F). Our failure to find any Msi-negative tumors in these mice coupled with our MSI

loss of function findings in human CRC cell lines strongly indicates that oncogenic Msi activity is required for the initiation and maintenance of intestinal cancers.

Msi1 Induction Phenocopies APC Loss and Transforms the Intestinal Epithelium

To determine the mechanisms by which Msi1 acts as an intestinal oncogene, we generated single copy, Doxycycline (Dox)-inducible, site-specific *Msi1* transgenic embryonic stem cell lines and mice (Beard et al., 2006; Kharas et al., 2010) and validated induction of Msi1 in response to Dox treatment (Figure 3A and S2A-C). Forty-eight hours after Dox administration in the drinking water of transgenic mice (*TRE-Msi1*) we observed strong expression of Msi1 throughout the small intestinal epithelium (Figure 3B, C). Strikingly, constitutive Msi1 activation resulted in a block in differentiation concomitant with a dramatic expansion of the crypt proliferative zone (Figure 3D-G). This differentiation block caused *TRE-Msi1* mice to become dehydrated, requiring euthanasia within 3-4 days of Dox administration. Goblet cells, enterocytes, and enteroendocrine cells were nearly completely absent 2 days after Msi1 induction (Figure 3D-F), however Paneth cells persisted, likely due to their long lifespan and stable positioning at the base of the crypt (Ireland et al., 2005) (Figure S2D). Strikingly, all of these phenotypes are consistent with acute loss of APC (Sansom et al., 2004). The stable positioning of Paneth cells at the crypt base in *TRE-Msi1* mice is the only phenotypic discrepancy between Msi1 induction and APC loss, as Paneth cells are mislocalized upon APC ablation (Sansom et al., 2004). We also examined the frequency of apoptotic cells and observed apoptotic events only at the tip of the villi in *TRE-Msi1* mice, consistent with increased shedding of cells into the lumen in response hyperproliferation in the crypt (Figure 3H). In addition to increased proliferation and crypt expansion, we also observed a striking increase in crypt fission, a phenomenon known to occur in response to *APC* inactivation (Wasan et al., 1998) (Figure 3I). Consistent with this observation, Msi1 was observed in $Lgr5^{+}$ crypt base columnar (CBC) stem cells at sites of crypt fission in wildtype mice (Figure 3J). These findings demonstrate that Msi1 activation closely phenocopies many of the features of *APC* loss in the intestinal epithelium, including increased proliferation, crypt fission, and a block in differentiation (Sansom et al., 2004).

Msi1 RNA Binding Activity Integrates Growth Control, Differentiation, and Signal Transduction Cascades.

To gain insight into pathways through which Msi1 functions, we performed transcriptome profiling of total intestinal epithelium (including both crypts and villi) 24 hours after Dox administration to *TRE-Msi1* or control (*M2rtTA)* mice, a timepoint just prior to the earliest onset of phenotypic change (Figure 4A and Table S1). We initially performed Gene Set Enrichment Analysis (GSEA)(Subramanian et al., 2005) against the C2 curated database and found 142 gene sets enriched at a nominal p value <0.01 in *TRE-Msi1* relative to control, and 103 gene sets enriched at a nominal p value <0.01 in control relative to *TRE-Msi1* (Table S2). Consistent with our histological observations, the most enriched signatures upon Msi1 activation were the *APC* loss gene signatures (Figure 4B). Genes that are activated upon *APC* loss are also activated upon Msi1 induction (the 11th most significant of 142 gene sets), and genes suppressed upon *APC* loss were similarly suppressed by Msi1 induction (the first and second most significant of 103 gene sets), and these changes were highly significant (Figure 4B and Table S2). Further, Msi1 induction also resulted in highly significant enrichment of gene signatures associated with RNA processing and translation, consistent with its known role as a cytoplasmic translational regulator that interacts with translational machinery (Kawahara et al., 2008) (Figure 4C and Table S2)

While transcriptome profiling provides insight into the pathways affected by Msi1 activation, it may not identify direct targets of Msi1 RNA binding activity as Msi1-mRNA interactions do not affect steady-state levels of known target mRNAs including *Numb* and *Cdkn1a* (Battelli et al., 2006; Imai et al., 2001; Kawahara et al., 2008). Therefore, to identify direct Msi1 RNA biding targets *in vivo,* we developed a method for performing CLIP-Seq (UV-crosslinking of Msi1-bound RNA followed by immunoprecipitation, RNAse digestion of unprotected regions, and massively parallel sequencing)(Ule et al., 2003) on purified, primary wildtype intestinal crypts and Msi1-transformed intestinal epithelium. Msi1 bound 2,371 transcripts in wildtype crypts, and ectopic Msi1 in *TRE-Msi1* epithelium bound 9,626 transcripts (Figure 4D and Table S3). The vast majority (93%) of Msi1 bound transcripts in WT crypts were also bound upon Msi1 induction. These binding events occurred primarily in 3'UTRs in wildtype crypts, consistent with the known function of Msi1 in translational suppression via interaction with consensus motifs in these regions (Figure 4D). There was significant binding of both coding and intronic sequences in wildtype crypts as well, however the biological significance of these events remains unclear. Ectopic expression of Msi1 increased binding of intronic sequences, and of the 7,422 transcripts bound only in *TRE-Msi1* epithelium, the vast majority (6,761, or 91%), were bound exclusively in their introns (Figure 4D, E), suggesting that ectopic Msi1 may saturate binding sites in available 3'UTR/CDS, resulting in promiscuous intronic binding.

Motif analysis indicated that Msi1 binds largely distinct sequences in introns and coding sequences in comparison to 3'UTRs, and although Msi1 binding motifs were A-U rich sequences, the previously described Msi1 motif discovered by an *in vitro* SELEX-based approach [(A/U)$U_{1\text{-}3}$AGU] (Imai et al., 2001) was not among the most significant (Figure 4F). This motif was, however, significant in the dataset and was located in the center of sequence reads containing this motif, demonstrating that it is indeed a *bona fide* motif *in vivo* (Figure S3A). Examination of the expression levels of Msi1 bound genes showed no preference for highly abundant transcripts, and transcripts newly bound upon induction of Msi1 exhibited no change in their expression levels on average (Figure S3B, C). These findings indicate that Msi1 binding does not globally affect target mRNA stability and support prior studies demonstrating that Msi1-mRNA interactions do not affect steady-state levels of *Numb* and *Cdkn1a* mRNAs (Battelli et al., 2006; Imai et al., 2001; Kawahara et al., 2008). We further confirmed the sequence-specific Msi1-RNA interaction by performing *in vitro* binding assays by incubating recombinant human MSI1 with RNA oligos containing the consensus motifs identified by CLIP (Figure S3D).

We examined binding of Msi1 to mRNA targets that had previously been identified after Msi1 overexpression *in vitro* (Battelli et al., 2006; Imai et al., 2001): *Cdkn1a* (encoding p21) and *Numb* mRNAs were both bound in *TRE-Msi1* epithelium, however these binding events were not significant in wildtype crypts, suggesting that during normal homeostasis, Msi1 may bind these targets infrequently or in a rare cell population (Figure 5A and S4A). We verified the functional consequences of Msi1 binding at the *Numb* 3'UTR upon Dox induction. Numb is a primary negative regulator of the Notch signaling pathway where it promotes the degradation of the Notch intracellular domain (NICD). Consistent with Msi1 acting as a translational suppressor, Msi1 knockdown in 293T cells resulted in increased activity of a luciferase-NUMB 3'UTR construct, and we observed a potent activation of the Notch pathway by cleavage and

accumulation of NICD and downstream induction of the Notch target gene *Hes1* in *TRE-Msi1* intestinal epithelium (Figure 5B and S3E). These findings confirm an established role for Msi1 in activating Notch signaling via *Numb* mRNA binding and can, in part, account for some of the increases in proliferation and block in differentiation observed in *TRE-Msi1* mice as Notch hyperactivation has been shown to elicit similar effects (Fre et al., 2005; Stanger et al., 2005).

Gene ontology analysis of CLIP targets revealed that Msi1 binds transcripts involved protein localization, possibly reflecting an established role in Msi1 governing asymmetric cell fate determination as has been observed for the Msi1 ortholog Musashi in *Drosophila* neuroblasts (Nakamura et al., 1994) and for MSI2 in hematopoietic stem cells (Kharas et al., 2010; Park et al., 2014) (Figure S3E). Msi1 binding targets function in a variety of pathways, most strikingly in the citric acid cycle, in adherens junctions, as well as in the Wnt signaling pathway. In addition to these major pathways, Msi1 also bound a number of mRNAs encoding functional proteins found in differentiated cells in the intestinal epithelium as well as established intestinal tumor suppressors, including *Lrig1* (Powell et al., 2012) and the transcripts encoding Mucins, Olfm4, and Lysozymes 1 & 2 (Figure S4A, and not shown). Thus, the pleiotropic inactivation of both tumor suppressors and differentiation genes may contribute to Msi1-induced phenotype.

Msi1 Drives an APC-Loss Transcriptional Program in the Absence of β-catenin Activation.
Based on our observation that the *TRE-Msi1* phenotype largely recapitulates that of acute *APC* loss, the identification of the Wnt pathway in Msi1 mRNA binding analysis, and the highly significant enrichment of *APC*-loss gene signatures in GSEA analysis (Figures 3, S3E, and 4B), we examined the status of the Wnt pathway in *TRE-Msi1* intestinal epithelium. Several *in vitro* studies recently suggested that Msi1 activation might support canonical Wnt pathway activity through direct binding and translational suppression of the *APC* mRNA (Rezza et al., 2010; Spears and Neufeld, 2011). We therefore examined Msi1 binding of *APC* mRNA in wildtype intestinal crypts and *TRE-Msi1* epithelium and observed a single binding peak in the 3'UTR (Figure 5C).

Since direct suppression of APC by Msi1 would provide an explanation of the observed phenotype in *TRE-Msi1* mice, we examined the expression of APC and β-catenin in the *TRE-Msi1* epithelium. Despite the observed binding of Msi1 to *APC* mRNA, we detected no loss of APC protein (Figure 5D and S4B), however it was still important to rule out hyperactivation of β-catenin transcriptional activity as a contributing factor to the *TRE-Msi1* phenotype. We therefore examined the presence of nuclear β-catenin in the crypts of *TRE-Msi1* mice. We observed no increase in nuclear β-catenin^{+} cells using 0.2mg/ml dox (a dose sufficient to induce full phenotypic penetrance and morbidity within 72-96 hours) (Figure 5E). Surprisingly, there was a near complete loss of nuclear β-catenin in cells of the crypt base at higher doses of dox (2mg/ml), which results in an identical phenotype to the 0.2 mg/ml dose (differentiation block and hyperplasia, Figure 5E, F).

Since high levels of Msi1 induction suppressed nuclear β-catenin accumulation, we examined the *Ctnnb1* 3'UTR in our CLIP dataset and observed strong Msi1 binding peaks, nearly an order of magnitude stronger than that of Msi1 binding to *APC* in *TRE-Msi1* epithelium (Figure 5G). We confirmed the relative binding of MSI1 to the *APC* and *CTNNB1* 3'UTRs in human cells using CLIP-qRT-PCR analysis in HEK293 cells and again observed approximately 10-fold greater

binding of MSI1 to *CTNNB1* relative to *APC*, consistent with our *in vivo* CLIP results (Figure S4C). Stimulation of canonical Wnt signaling in these cells by inactivation of the destruction complex with a GSK3-β inhibitor (CHIR) resulted in decreased MSI1 binding to these target mRNAs (Figure S4C). We confirmed that MSI1 was capable of suppressing translation via interaction with the *CTNNB1* 3'UTR, as MSI1 overexpression and knockdown in 293T cells resulted in the decreased and increased activity of a *CTNNB1* 3'UTR-Luciferase reporter, respectively (Figure S4D). We further confirmed that MSI1 is capable of suppressing canonical Wnt signaling via TOPflash reporter assays in HCT116 human colorectal cancer cells with constitutively active β-catenin (destruction complex phosphorylation site mutant) (Figure 5H). We also examined the expression of a number of known direct β-catenin binding targets in Tre-Msi1 intestinal epithelium and found no evidence for their increased expression upon Msi1 induction (Figure S4E).

To unequivocally demonstrate that Msi1 can drive proliferation in the absence of β-catenin, we crossed *TRE-Msi1* mice to *Ctnnb1*$^{flox/flox}$*::VillinCreERT2*, deleted *Ctnnb1*, then induced Msi1 expression with dox. In the absence of Msi1 induction, loss of β-catenin lead to loss of tissue integrity within 4 days of deletion as previously described (Fevr et al., 2007) (Figure 5I and S4F). In contrast, induction of Msi1 after *Ctnnb1* deletion clearly drove proliferation in the complete absence of nuclear β-catenin, although the proliferative zone was reduced in comparison to *TRE-Msi1* epithelium due to the lack of functional adherens junctions in the absence of β-catenin (Figure 5I and S4G). Taken together, these findings provide compelling evidence that, 1) Msi1 can act as a suppressor of canonical Wnt signaling in intestinal epithelial cells (although the biological relevance of this is unclear) and, 2) the phenotypic consequence of Msi1 activation occur in the absence of canonical Wnt pathway activation.

Msi1 Drives PI3K-AKT-mTORC1 Activation Downstream of Pten.

Based on our observations that Msi1 is able to drive crypt hyperplasia and fission and block differentiation in the absence of canonical Wnt pathway activation, along with the observation that Msi1 induction activates transcriptional programs associated with mRNA biogenesis, we examined the transcriptome profiling and CLIP data for Msi1 targets that may mediate these effects. We observed strong binding of Msi1 to the 3'UTR of the Pten tumor suppressor mRNA after Dox induction (Figure 6A). Pten is frequently inactivated in colorectal cancers, and deletion of Pten in the intestine initiates polyposis and drives crypt fission (phenotypes consistent with both *APC* loss and Msi1 induction)(Garcia et al., 2003; Goel et al., 2004; He et al., 2007). Pten is a well-known negative regulator upstream of the mTORC1 complex that, in turn, acts to drive mRNA biogenesis and translation. Consistent with Pten suppression and mTORC1 activation, GSEA revealed a strong inverse correlation between the *TRE-Msi1* gene signature and that of Rapamycin (Rap) treatment (i.e., genes suppressed by Rap are upregulated by Msi1 and those activated by Rap are suppressed by Msi1) (Figure 6B and S5A). Rapamycin is a potent inhibitor of the mTORC1 complex, and thus these findings further suggested that the mTORC1 complex was being activated downstream of Msi1. We therefore examined more closely the activity of the PI3K-AKT-mTORC1 signaling axis.

Analysis of Pten protein levels and S6 kinase (S6K) activity (a canonical mTORC1 target) after Msi1 induction revealed a decrease in Pten protein (consistent with translational repression by Msi1) and a concomitant increase in S6 phosphorylation by S6K (consistent with mTORC1

activation) (Figure 6C). Downstream of Pten inactivation, an increase in Pten enzymatic activity occurred upon MSI1 inhibition in 293 cells (Figure S5B). In TRE-Msi1 mice there was increased phosphorylation of AKT at T308 by PDK1 (PDPK1) (Figure 6D). AKT phosphorylation at S473 by mTORC2, however, showed only a minor increase, indicating that mTORC1 activation is due to increased AKT activity via activation of AKT by the PI3K pathway (Figure 6D). Consistent with this notion, we also observed an increase in the activating PDK1 autophosphorylation event at S241 (Figure 6D). We observed an increase in phosphorylation of the AKT target c-RAF (S259), further supporting the activation of AKT downstream of Msi1 induction. Downstream of mTORC1, there was strong inactivating phosphorylation of the translational inhibitor 4EBP1, resulting in activation of the translational initiation factor eIF4E (Figure 6D). Examination of the spatial distribution S6 kinase activity revealed a dramatic expansion, with activity normally restricted to the crypt expanded throughout the entire epithelium upon Msi1 induction (assessed by phosphorylation of S6, Figure 6E). We further confirmed that mTORC1 activation by Msi1 was β-catenin-independent in *TRE-Msi1::Ctnnb1*$^{flox/flox}$*::VillinCreERT2* mice, where Msi1 induces S6 phosphorylation after loss of β-catenin (Figure S4F,G and S5E)

We thus conclude that activation of the PDK1-AKT signaling axis downstream of Pten by Msi1 accounts for the observed increase in mTORC1 activity in the intestinal epithelium. We confirmed that the inhibitory effect of MSI on PTEN also occurred in human colorectal cancer cell lines. Analysis of phosphatidylinositol-3,4,5 triphosphate (PIP3), a readout for active receptor tyrosine kinase signaling and a substrate of PTEN, demonstrates that MSI knockdown decreases PIP3 at the plasma membrane of tumor cells, indicating increased PTEN activity (Figure 6F and S5C). Increased PTEN enzymatic activity was also observed upon MSI1/2 knockdown using an immunoprecipitation-ELISA assay (Figure S5D). Thus, the effects of TRE-Msi1 induction on the murine intestinal epithelium through Pten inhibition are conserved to the oncogenic Msi1 expression in human CRC.

While Msi1 activation potentially has pleiotropic oncogenic effects including inactivation of tumor suppressors such as Lrig1, Numb and p21 and suppression differentiation, our data suggests that the activation of mTORC1 and the downstream consequences thereof may be a primary mediator of the *TRE-Msi1* phenotype. We therefore treated *TRE-Msi1* mice with the mTOR inhibitor Rapamycin for several days prior to induction of Msi1 with Dox. This resulted in a decrease in mTORC1 activity (determined by S6 phosphorylation, Figure S5E) and concomitant rescue of the *TRE-Msi1* phenotype, including a significant decrease in crypt fission, proliferation, and crypt height expansion (Figure 6G-I). These findings demonstrate that mTORC1 activation plays a key functional role in Msi1-induced phenotypic alterations of the intestinal epithelium.

Msi1 Drives Quiescent Stem Cell Activation

In mice, APC loss initiates tumorigenesis only when it occurs in an intestinal stem cell; either the actively cycling Lgr5^{+} crypt base columnar ISC, or the reserve, more quiescent ISC marked by a *Bmi1-CreER* knockin allele (Barker et al., 2009). Further, mTORC1 inhibition with Rapamycin abrogates tumorigenesis upon APC loss (Fujishita et al., 2008; Koehl et al., 2010). These observations, coupled with observations that Msi1 is expressed in ISCs and Msi1 induction

drives a common stem cell gene signature (Ramalho-Santos et al., 2002) (Figure 7A) suggested that the primary effects of Msi1 might occur within the stem cell compartment. We hypothesized that the Msi1-induced hyperproliferation and block in differentiation were a consequence of the replacement of differentiated cells in the villi with undifferentiated stem/progenitor cells originating from the crypt. Therefore we examined the fate of Lgr5$^+$ cells in *TRE-Msi1::Lgr5-eGFP-IRES-CreER* compound mice after Dox induction and observed an expansion of *Lgr5-eGFP*$^+$ zone towards the top of the intestinal crypts and an increase in the frequency of *Lgr5-eGFP*$^+$ cells, indicating that Msi1 drives expansion of the undifferentiated stem cell compartment (Figure 7B-C). Consistent with this notion, withdrawal of Dox resulted in a reversion to a normal homeostatic epithelium that persisted >6 months, demonstrating that long-term stem cells are retained after Msi1-induction (Figure 7D). We next verified that effects of Msi1 were epithelial cell-autonomous by purifying intestinal crypts from *TRE-Msi1::Lgr5-eGFP-IRES-CreER* mice, initiating organoid cultures (Sato et al., 2009), and inducing Msi1 expression by addition of Dox *in vitro*. Similar to our *in vivo* findings, Msi1 induction drove robust budding and elongation of *Lgr5-eGFP*$^+$ crypts originating from a common, central lumen (Figure 7E).

The observed expansion of *Lgr5-eGFP*$^+$ ISCs upon Msi1 induction could be accounted for by either an Lgr5$^+$ cell-intrinsic proliferative effect, or by the promiscuous activation of the more quiescent, reserve stem cells that in turn, give rise to progeny that pass through an *Lgr5-eGFP*$^+$ state. The reserve ISC is much slower cycling than the Lgr5$^+$ cell and gives rise to Lgr5$^+$ cells at low frequency during homeostasis, and much more frequently during regeneration after injury (Sangiorgi and Capecchi, 2008; Tian et al., 2011; Yan et al., 2012). We therefore sought to address the effects of Msi1 activation on these reserve stem cells. Reserve, or +4 ISCs are marked by knockin reporter alleles at the *Bmi1* locus (Sangiorgi and Capecchi, 2008; Tian et al., 2011; Yan et al., 2012), however the presence of the endogenous Bmi1 mRNA is distributed throughout the crypt (Itzkovitz et al., 2012), highlighting discrepancies between gene activity and mRNA distribution and generating some controversy as to the identity of the active versus reserve ISC populations. Despite this controversy, the *Bmi1-CreER* knockin is the only reporter allele that has been functionally demonstrated to mark a radio-resistant, slow cycling intestinal stem cell capable of giving rise to Lgr5+ ISCs (Sangiorgi and Capecchi, 2008; Tian et al., 2011; Yan et al., 2012). Further, *in vivo* cell ablation experiments demonstrated that unlike Lgr5+ ISCs, the *Bmi1-CreER*-marked ISCs are indispensible for intestinal homeostasis, indicating that this knockin allele marks the master, reserve intestinal stem cell (Sangiorgi and Capecchi, 2008; Tian et al., 2011; Yan et al., 2012).

We initially assessed the effect of Msi1 on the frequency of *Bmi1-CreER*+ ISCs using a *Bmi1-CreER::Lox-Stop-Lox-tdTomato* reporter allele, sorted 18hrs after reporter activation (hereafter referred to as *Bmi1-Tomato*$^+$) (Sangiorgi and Capecchi, 2008; Tian et al., 2011; Yan et al., 2012). Treatment of *TRE-Msi1* mice with dox for 48 hours resulted in a marked increase in the frequency of the *Bmi1-Tomato*$^+$ population (Figure 7F), suggesting that the primary effects of Msi1 induction may, in fact, be upstream of the Lgr5+ crypt base columnar stem cell at the level of the reserve, *Bmi1-Tomato*$^+$ ISC.

To directly address this point, we examined the immediate early consequences of Msi1 activation in these two populations 24 hours after dox administration (prior to any morphological

alterations) at the single cell level using Fluidigm Biomark HD dynamic arrays. We analyzed the expression of 48 genes in single *Lgr5-eGFP+* and *Bmi1-CreER+* stem cells in either the presence or absence of Msi1 induction (Figure S6A). As expected, *Lgr5-eGFP+* cells exhibited high levels of proliferative and Wnt pathway-related genes, and expressed Bmi1, consistent with previous reports describing the presence of this putative reserve stem cell transcript in active crypt base columnar stem cells (Itzkovitz et al., 2012; Munoz et al., 2012) (Figure 7G, H and S6A). In contrast, the *Bmi1-Tomato*$^+$ stem cells comprised a heterogeneous population; the majority of these cells had no expression of Lgr5, and overall low expression of Wnt, Notch, and proliferation related genes (Figure 7G, H and S6A, B), consistent with their being a transcriptionally silent, relatively quiescent stem cell. A subset of *Bmi1-Tomato*$^+$ cells (less than 10%) had begun to activate Lgr5, Wnt, Notch, and proliferation related genes (Figure 7H and S6A, B). Principal component analysis (PCA) indicates that this subset of *Bmi1-Tomato*$^+$ cells have an *Lgr5-eGFP*-like identity (Figure 7G). These findings demonstrate that the *Bmi1-Tomato* knockin reporter labels primarily a distinct, reserve stem cell population along with a subset of cells undergoing activation to an Lgr5$^+$ crypt base columnar state.

Having established baseline gene expression patterns in these two stem cell types, we next analyzed these same populations 24 hours after induction of *TRE-Msi1*. Strikingly, Msi1 induction had no discernable effect on the expression pattern or PCA clustering of *Lgr5-eGFP*$^+$ cells (Figure 7G, H and S6A, B). In stark contrast to the *Lgr5-eGFP*$^+$ cells, the *Bmi1-Tomato*$^+$ reserve stem cells exhibited robust gene activation upon Msi1 induction, including dramatic activation of genes downstream of mTORC1 activity, *Hif1α* and *Hexose-6-Phosphate Dehydrogenase* (*H6PD*, an important enzyme in the pentose phosphate pathway downstream of mTORC1, (Duvel et al., 2010)(Figure 7G-H). Msi1 also induced expression of Amphiregulin and Epiregulin, two mitogenic ErbB receptor ligands that may also contribute to mTORC1 pathway activation, as ErbB receptors are known to activate mTORC1 in cancer cells (Koziczak and Hynes, 2004; Zhou et al., 2004) (Figure S5). Examination of Wnt pathway gene expression in Msi1-induced reserve stem cells revealed no activation of canonical Wnt targets *Ascl2* and *Axin2,* and few cells activating *Lgr5* (Figure 7H and S6A, B). These findings demonstrate that the immediate early effect of Msi1 induction is activation of the reserve stem cell compartment into a state that is distinct from that of the normal CBC stem cell (Figure 7G).

We next verified activation of the mTORC1 pathway at the protein level in *Bmi1-Tomato*$^+$ and *Lgr5-eGFP*$^+$ cells at a later timepoint (36 hours after Msi1 induction). In control mice, *Lgr5-eGFP*$^+$ cells had a higher basal level of pS6, which was undetectable in control *Bmi1-Tomato*$^+$ cells, consistent with their primarily quiescent state (Figure 7I). Thirty-six hours of Dox induction resulted increased S6 phosphorylation in both of these populations, consistent with Msi1 driving mTORC1 activation (Figure 7I).

Ultimately, we directly compared the effects Msi1 activation in *Bmi1-Tomato*$^+$ and *Lgr5-eGFP*$^+$ cells with the effects of active β-catenin (S33) induction in crypts after 48 hours of dox induction. For this we utilized an analogous mouse model to our *TRE-Msi1* model in which a non-degradable form of β-catenin is targeted as a single copy under control of the tetracycline responsive element in loci identical to those used in *TRE-Msi1* in genetically identical mice (*TRE-β-cat-S33*) (Hirata et al., 2013). Activation of *Myc*, *Hif1a*, Hif2a (*Epas1*), and *H6PD*, but not Wnt targets *Ascl2*, *Axin2*, or *Lgr5* was observed in both *Bmi1-Tomato*$^+$ and *Lgr5-eGFP*$^+$

ISCs 48 hours after Msi1 induction (Figure 7J). In contrast, 48 or 96 hours of β-catenin-S33 activation strongly induced *Ascl2*, *Axin2*, and *Lgr5*, but not *Hif1a*, Hif2 (*Epas1*), or *H6PD* . Further, histological analysis of *TRE-β-cat* mice revealed an increase in crypt height, similar to Msi1 induction and APC loss. However, unlike *TRE-Msi1* induction and APC loss, *TRE-β-cat* exhibited no increase in crypt fission nor block in differentiation *in vivo*, even after 96 hours of dox exposure (Figure S6). These findings support a model in which the β-catenin and Msi1 activate distinct pathways in ISCs that cooperate to drive transformation of the intestinal epithelium and the progression of colorectal cancers.

In this study we reveal that the oncogenic activity of Msi proteins is required for tumor initiation resulting from LOH of the APC tumor suppressor in mice and for the *in vitro* and *in vivo* growth of human colorectal cancer cells. We identify Msi1 as an oncogene whose constitutive activation alone is sufficient drive the activation of reserve intestinal stem cells, block the differentiation of this expanded pool of undifferentiated cells, and induce crypt fission Remarkably, our findings demonstrate that Msi1 can elicit these effects without activating the canonical Wnt pathway/β-catenin. Instead, Msi1 binds to transcripts that encode an array of well-known intestinal tumor suppressors including Numb, p21, Lrig1, and Pten. Msi1 activation results in decreased Pten protein and activity levels, subsequently activating the AKT-mTORC1 axis. Interestingly it has previously been established that mTORC1 activation is required for adenoma formation upon APC loss (Fujishita et al., 2008). In keeping with this model, we find that mTORC1 activation is similarly required for the phenotypic changes we observe upon Msi1 activation including crypt hyperplasia and crypt fission, and in turn that Msi activity is required for adenoma formation upon APC loss. These findings suggest that Msi activity may represent an unrecognized oncogenic pathway that cooperates with canonical Wnt signaling to drive intestinal tumorigenesis.

Further evidence for this notion comes from the comparison of the effects of Msi1 induction to those of β-catenin. A plethora of evidence indicates that β-catenin activity is required for intestinal tumorigenesis, and that β-catenin activation drives the expansion of a crypt-base-columnar intestinal stem cell gene expression program (Merlos-Suarez et al., 2011; van de Wetering et al., 2002). Our findings with an inducible β-catenin mouse model support this notion as we observe a strong induction of canonical Wnt target genes upon β-catenin activation, including *Lgr5*, *Axin2*, and *Ascl2*. β-catenin activation in this mouse model results in a crypt hyperplasia similar to what we observed upon Msi1 activation. Unlike Msi1 activation however, β-catenin induction did not drive crypt fission nor elicit a strong block in differentiation. Thus, Msi1 activation elicits a phenotypic response that is distinct from that of β-catenin.

Interestingly, recent studies targeting *APC* loss (which results in activation of both β-catenin and Msi1) in specific cell types of the intestinal epithelium have revealed that only cells with self-renewal capacity (either reserve +4 or cycling crypt base columnar stem cells) are susceptible to this oncogenic insult (Barker et al., 2009). This led us to investigate the effects of Msi1 induction on these intestinal stem cell populations. We initially observed an expansion of *Lgr5-eGFP+* cells in response to Msi1 induction. This finding could be accounted for by either an increase in the intrinsic proliferation of the active, crypt base columnar stem cells, or by the promiscuous activation of the reserve, primarily quiescent intestinal stem cell. A number of recent studies have provided compelling evidence for the existence of this functionally distinct,

radioresistant reserve intestinal stem cell population using a *Bmi1-CreER* knockin reporter allele. Cells marked by this allele are capable of giving rise to all differentiated intestinal cell types including the generation Lgr5+ cells during both homeostasis and regeneration (Sangiorgi and Capecchi, 2008; Tian et al., 2011; Yan et al., 2012). Remarkably, the actively cycling Lgr5+ stem cells are dispensable for intestinal homeostasis, whereas ablation of *Bmi1-CreER* reserve stem cells results in crypt loss and failure of the epithelium (Sangiorgi and Capecchi, 2008; Tian et al., 2011; Yan et al., 2012). These studies elegantly demonstrate that *Bmi1-CreER* marks a master, slow cycling, reserve intestinal stem cell.

When we examined the immediate effects of Msi1 induction on the transcriptional activation of the *Lgr5-eGFP*$^{+}$ crypt base columnar ISC compared to the *Bmi1-CreER*$^{+}$ reserve ISC, we strikingly found that Msi1 selectively drove the activation of the reserve stem cells while having little effect on the CBC transcriptional program. Remarkably, Msi1 does this without activating canonical Wnt target genes such as *Ascl2*, *Axin2*, or *Lgr5*. Rather, Msi1 drives mTORC1 activation in these reserve cells, along with the expression of oncogenic genes such as *Amphiregulin*, *Epiregulin*, *Myc*, and *Hif1a*. Our observations that Msi loss abrogates adenoma formation in the *APC*$^{min/+}$ mouse lead us to speculate that promiscuous activation of the reserve intestinal stem cell population may play a critical role in intestinal tumorigenesis, in addition to the proliferative expansion of the *Lgr5-eGFP*$^{+}$ stem cell. It is tempting to further speculate that Msi1 and β-catenin cooperate to simultaneously achieve both of these effects during adenoma formation: Msi1 activates reserve intestinal stem cells through mTORC1 activation, then β-catenin drives the expansion of *Lgr5-eGFP*$^{+}$ stem cell and the canonical Wnt gene expression program. Further studies are required to definitely test such a model, however if this is the case, dual inhibition of Wnt and Msi activity may provide a potent anti-tumorigenic effect. Indeed, this notion is supported by our loss of function experiments in human colorectal cancer cells, where inhibition of Msi or β-catenin each provide some growth inhibition, while combined Msi and β-catenin inhibition completely abrogate tumor growth. Thus, the highly conserved MSI RNA-binding domain may be a viable target for pharmacological inhibition to aid in reactivation of tumor suppression in combination with β-catenin and mTORC1 inhibitors for the treatment of colorectal adenocarcinomas.

Experimental Procedures

Generation of Dox-inducible Msi1 Mice

The murine *Msi1* cDNA (a kind gift from Dr. Joseph Verdi, Maine Medical Center Research Institute) was cloned into the unique *EcoRI* restriction site of the pBS31 vector containing a *PGK* promoter followed by an ATG start codon and an FRT recombination site, followed by a splice acceptor-double polyA cassette, the tetracycline operator with a minimal CMV promoter, the unique *EcoRI* site, and an SV40 polyadenylation signal. The pBS31-Msi1 vector was then electroporated along with a Flpe recombinase-expressing vector into KH2 embryonic stem cells harboring the modified reverse tetracycline transactivator (*M2rtTA*) targeted to and under transcriptional control of the *ROSA26* locus, as well as an FRT-flanked *PGK-neomycinR* cassette followed by a promoterless, ATG-less hygromycinR cassette targeted downstream of the *Collagen1a1* locus. Selection for hygromycin resistance upon flip-in yielded numerous colonies which were verified for proper recombination at the Coll1a1 locus by digestion of genomic DNA and Southern blotting with a 3' internal probe, yielding a 6.2kb wildtype band, a 6.7kb band for

the FRT-containing knock-in allele, and a 4.1kb band for the successfully flipped-in Msi1 inducible allele (*TRE-Msi1*).

Doxycycline Induction and Isolation of Intestinal Epithelium

For Dox induction of control (*M2rtTA* alone), *TRE-Msi1* mice, and *TRE-β-catenin-S33* mice, 0.2-2.0 mg/mL of Dox (Doxycycline hyclate, Sigma) was added to the drinking water along with 1% w/v sucrose of mice 2-3 months of age. For isolation of intestinal epithelial cells, mouse intestine was cut longitudinally and washed 2-3 times with ice-cold PBS, then cut into small pieces (1 cm long) and incubated for 1 hour at 4 °C in PBS containing 2 mM EDTA and 0.2 mM DTT on a rotating platform. Intestinal epithelial cells were released by vortexing. For isolation of intestinal crypts, mouse small intestine was isolated and rinsed in PBS as above. The villi were scraped using a hemocytometer coverslip. The crypts were released from murine small intestine by incubation for 30 min at 4 °C in PBS containing 2 mM EDTA. Isolated crypts were counted and pelleted as described in (Sato et al., 2009).

Administration of Rapamycin

Rapamycin (LC Laboratories) was administered by daily intraperitoneal injection (4 mg per kg of body weight) for 5 days. It was reconstituted in absolute ethanol at 10 mg/ml and diluted in 5% Tween-80 (Sigma) and 5% PEG-400 (Hampton Research) before injection. The final volume of all injections was 200 ul. Dox was administered to *TRE-Msi1* mice for 48hours after the third dose of Rapamycin prior to euthanasia.

Histology, Immunofluorescence, and Immunochemistry

All histological analysis was performed on 3 or more individual mice, and controls and experimental groups were either sex-matched littermates or age-matched, sex-matched non-littermates. We observed no histological differences between TRE-Msi1, M2rtTA, and WT mice in the absence of doxycycline. Intestines were washed with PBS, fixed in 10% Formalin, paraffin-embedded and sectioned. Hematoxylin, eosin, Alcian blue, and Alkaline Phosphatase staining was performed in the Morphology Core of the Penn Center for Molecular Studies in Digestive and Liver Diseases. For immunohistochemistry staining, antigen-retrieval was performed by heating slides in 0.01 M citrate buffer (pH 6) with a pressure cooker. The sections were then immunostained by the ABC peroxidase method (Vector labs) with diaminobenzidine (DAB) as the enzyme substrate and hematoxylin as a counterstain. For detection of nuclear β-catenin, antibody clone 15B8 (Sigma; 1:1000) was used in combination with the MOM kit (Vector Laboratories). For immunofluorescence staining, paraffin sections were pretreated in 0.01 M citrate buffer (pH 6) with a pressure cooker, and incubated in primary antibodies, then incubated with Cy2- or Cy3- conjugated fluorescent secondary antibodies (Jackson Laboratory) and counterstained with DAPI in mounting media (Vector labs). The following antibodies were used: Ki67 (Leica), Msi1 (MBL), Lysozyme (Santa Cruz), Chromogramin A (Abcam), GFP (Abcam), and APC (Santa Cruz C-20). Msi1 and Lgr5 positive cell position was analyzed based on 100 randomly selected crypts as described previously (Barker et al., 2007) (Figure 1D). Crypt numbers per 1 mm were counted based on 25 randomly selected areas (Figure 3I). Nuclear β-catenin positive cell numbers per crypt were based on 2 independent experiments and 75 randomly selected crypts (Figure 5E). Crypt numbers per 1 mm were counted based on 20 randomly selected areas in proximal and distal intestine (Figure 6G), crypt height was measured based on 40 crypts (Figure 6H) (n=3 independent pairs of mice).

For analysis of *TRE-Msi1* effects in a β-catenin null background, we crossed *TRE-Msi1* mice to *Ctnnb1*$^{flox/flox}$ mice with a *VillinCreERT2* allele. *Ctnnb1* was deleted by 2 consecutive daily doses of Tamoxifen (2 mg each), followed by administration of Dox 72 hours after the initial tamoxifen dose. Mice were continually treated with Dox for an additional 48 hours followed by tissue isolation and processing, resulting in an endpoint 5 days after *β-catenin* ablation and 48 hours after Msi1 induction.

CLIP-Seq and CLIP-qRT-PCR

CLIP-Seq libraries were made as previously described in (Chi et al., 2009) with modifications. Total intestinal epithelial cells from two individual *TRE-Msi1* mice treated with Dox for 24 hours were isolated as above, and wildtype intestinal crypts from two control mice were isolated as above. For crosslinking, cell suspension was exposed to 2 pulses of 265nm UV light at 400mJ/cm^2 in a Stratalinker (Model 2400, Stratagene). Epithelial cells were then lysed using PXL buffer (PBS, 01% SDS, 0.5% deoxycholate, 0.5% NP-40, plus protease inhibitor and RNAsin). The lysates were sequentially treated with DNaseI and RNase, and spun in ultra-microcentrifuge at 40,000g for 20 min. The supernatant was added to protein A Dynabeads (Dynal, 100.02) conjugated with Msi1 antibody (AB5977, Millipore) and incubated for 4 hours at 4 °C. ^{32}P-γ-ATP labeled 3' RNA (RL-3) linker was ligated to the RNA fragment on beads overnight at 16°C. The beads were re-suspended in 30 μl of Novex loading buffer (without reducing agent), and separated with Novex NuPAGE 10% Bis-Tris gel and transferred to S&S BA-85 nitrocellulose membrane. After overnight exposure, around 50 KD band was visualized and the corresponding membrane was cut to small pieces. The RNA was released by proteinase K digestion and isolated using RNA phenol and $CHCl_3$ solution. 5' RNA (RL-5) linker was ligated into the RNA fragments. The RNA was transcribed into complementary DNA using RT-PCR and amplified using Re-PCR with Solexa fusion primers. The CLIP library underwent single-end sequencing on an Illumina hiSeq2000 at the University of Pennsylvania Functional Genomics Core. RL-3: 5'-OH GUG UCA GUC ACU UCC AGC GG 3' –puromycin; RL-5: 5' –OH AGG GAG GAC GAU GCG G 3'-OH. Adaptor sequences ('GTGTCAGTCACTTCCAGCG') were removed from the 3' end using the fastx-toolkit (http://hannonlab.cshl.edu/fastx_toolkit/). Reads were then mapped using Bowtie (-k 100 -n 0) to the mouse genome (mm9) (Langmead et al., 2009). Peaks were then called using an FDR ≤ 0.05 and motifs were identified using Homer (http://biowhat.ucsd.edu/homer/). The peaks were then annotated using a set of customized Perl and R scripts. GEO accession numbers for CLIP-Seq datasets are pending.

For CLIP-qRTPCR, HEK 293 cells treated with GSK3β inhibitor or untreated control were crosslinked and immunoprecipitated with anti-MSI1 antibody as above. Immunoprecipitated RNA was subjected to quantitative RT-PCR analysis after reverse transcription using a first strand synthesis kit (Invitrogen) and primers specific to the 3'UTRs of *APC* or *CTTNB1* in an ABI Prism quantitative PCR machine using standard 2 stage cycling protocols and SYBR green detection (n=3 biological replicates).

Transcriptome Profiling

Total RNA was isolated from total mouse small intestinal epithelial cells from 3 *M2rtTA* and 3 *TRE-Msi1* mice administered Dox for 24 hours in the drinking water using TRIzol Reagent (Life

Technologies) according to the manufacturer's instructions. Total RNA was DNAse treated with an RNAse-free DNAse kit (Zymo Research). Purified RNA was submitted to the University of Pennsylvania Molecular Profiling Core, where samples were labeled and hybridized to Affymetrix Mouse Gene 1.0ST arrays. Microarray data was analyzed using Partek® Genomics Suite™ software. Following RMA background subtraction and normalization, a 1-way-ANOVA analysis between controls (*M2rtTA*) and Msi1 induced (*TRE-Msi1*) was run to compute *p-values* of significance and *F-statistic* for each probeset. *q-value*, a measure of false discovery rate (FDR) was computed within the SAM (Significance Analysis of Microarrays) software for each probeset by running an unpaired *t-test*. The FDR values were integrated with the 1-way-ANOVA results. Genes that were significant at FDR cut-off of 5% and changed at least 2-fold in either direction in the Msi1 induction group when compared to the control group were selected as the set of differentially expressed genes. This set of 836 unique genes and 6 samples were subjected to agglomerative hierarchical clustering analysis. Log2 intensities were median-centered across samples. Euclidean distance was used as the dissimilarity metric and average linkage method as clustering strategy. Results were visualized as intensity heatmap (Figure 4A). GEO accession numbers for microarray datasets are pending.

For analysis of direct β-catenin target gene expression in Figure S4E, genes with published evidence for direct regulation by β-catenin demonstrated by chromatin immunoprecipitation were selected. These genes include *Edn1, Fra-1 (Fosl1), c-Myc, Met, c-Jun, Pinx1, Tcf4, Egfr, Klf5, Cyclin D (Ccnd1), Mycbp, Mmp7, Cdkn2a, Vegfa, SNAI1, Fgf18, Gja1 (connexin-43), Axin2, Claudin1, Runx2, Lef1, Bglap, ENPP2, Nrcam, DLK1, Vcan, Fgf4, Fn1, Tcf1, (Hnf1a), Lgr5, Ppard, Sp5, Ovol1, Id2, L1CAM, Cdh1 (E-cadherin), Fst, Tnfrsf19, Neurod1, Ctla4, Wisp1, Fzd7, Mitf, Pou3f2, Gbx2, Nkx2-2, Neurog1, Eda, T, Pitx2, Btrc, Cdx1, Birc5 (survivin), Pkd1, Pml, and Lect2 (chemotaxin2).*

Flow Cytometry, Single-Cell Sorting, and qRT-PCR on Sorted ISC Populations

The intestine was cut open longitudinally and incubated with 5mM EDTA-HBSS solution at 4°c for 30min. Single cell suspension was generated with Accutase (BD Biosciences, San Jose, CA). Flow cytometry analysis was performed with BD LSRFortessa cell analyzer (BD Biosciences, San Jose, CA). DAPI negative cells were selected, then gated for single cell based on Forward-scatter height versus forward-scatter width (FSC-H vs FSC-W) and side-scatter height vs side-scatter width (SSC-H vs. SSC-W) profiles. Single-cell sorting experiments was performed with BD FACSAriaII cell sorter, each single cell was sorted into a different well of a 96-well PCR plate, using the FACSAriaII flow cytometer software package (FACSDiva) with single cell precision mode. The size of the nozzle for all sorting is 100 μm (20 psi).

Lgr5+ stem cells were quantified by flow cytometry and isolated by FACS from *TRE-Msi1::Lgr5-eGFP-IRES-CreER* and *M2rtTA::Lgr5-eGFP-IRES-CreER* control mice after 48 hours of Dox treatment. Bmi1+ stem cells were isolated from *TRE-Msi1::Bmi1-CreER::Lox-Stop-Lox-tdTomato* and *M2rtTA::Bmi1-CreER::Lox-Stop-Lox-tdTomato* control mice. These mice were induced with Doxycycline for 30 hours, then treated with Tamoxifen to activate tdTomato expression in Bmi1 expressing cells, then were euthanized after an additional 18 hours of Dox treatment (total 48 hours Dox). 20,000 Lgr5+ or Bmi1+ cells were purified from control (*M2rtTA* only) and experimental (*TRE-Msi1*) mice and subjected to qRT-PCR analysis as described.

Two-Step Single-Cell Gene Expression

The Two-Step Single-cell gene expression protocol (advanced development protocol 33) from Fluidigm was adopted in this experiment. Briefly, 5 µL of RT Mix Solution which includes 1.2 µL 5X VILO™ Reaction Mix (Life Technologies, 11754-250), 0.3 µL SUPERase-In (Life Technologies, AM2696) and 0.25 µL10% NP40 (Thermo Scientific, 28324) was dispensed into each well of 96-well-plate. One single cell was sorted into the well directly. The plate was vortexed briefly and immediately frozen on dry ice. When ready to perform RT cycling, the plate was thawed on ice and RNA denatured by incubating the plate at 65 °c for 90 sec then chilled on ice for 5 min. Each well was supplemented with 1 µl mixture of 10X SuperScript® Enzyme Mix (Life Technologies, 11754-250) and T4 Gene 32 Protein (New England BioLabs, PN M0300S). The mRNA was reverse transcribed into cDNA following the thermal cycling conditions below: 25°c, 5 min/ 50°c, 30 min/ 55°c, 25 min/60°c, 5 min/ 70°c, 10 min. The resulting cDNA was pre-amplified with 50 nM primer mix for 23 PCR cycles (96 °c for 5 sec, 60 °c for 4 min) (STA step) and then treated with ExoI for 30 min to remove unincorporated primers. The final product was diluted 1:3 with TE buffer. For each chip sample inlet, 2.25 µl diluted cDNA, 2.5 µl 2X Sso Fast EvaGreen supermix with low ROX and 0.25 µl of Fluidigm sample loading agent were added. Individual gene-specific DELTAgene assay were diluted at 1:10 ratios with TE buffer. 2.5 µl of each primer was then mixed with 2.5 µl assay loading agent inserted into the chip "assay" inlets. The manufacturer's instruction to perform chip loading and RT-PCR was followed. The data were analyzed in the Fluidigm Gene Expression Analysis Package. All primer sequences used in Fluidigm analysis are available on request.

Violin plots were generated form data consisting of 47 cells in the Bmi1 condition, 48 cells in the Bmi1+Msi1 condition, 43 cells in the Lgr5 condition and 43 cells in the Lgr5+Msi1 condition. For each cell, we have a measure of the cycle time for 96 primer sets (48 genes with duplicate primer sets). A cycle value of 30 was imputed for any cycle values that did not amplify by 30 cycles (i.e., no signal). For each gene, violin plots were constructed using the statistical software R to compare the distribution of cycle times for that gene between the four conditions (Bmi1, Bmi1+Msi1, Lgr5 and Lgr5+Msi1). For PCA analysis, Fluidigm Ct values were averaged for each gene (across the two primer sets per gene) in each sample. Principal Components Analysis (PCA, using Partek Genomics Suite v6.6, Partek, Inc. St. Louis, MO) was used to visualize the global variation across the samples. Samples were colored to represent their condition.

Reporter Assays

HCT116 cells were plated in 24-well-plate and transfected, in triplicate, with 0.5µg reporter vector (TOPflash Wnt reporter, FOPflash control reporter) together with 0.5µg of the human MSI1 expression vector (in pCDNA6) using FUGENE 6 transfection reagent (Promega). 48h after transfection cells were harvested for reporter assay using the Dual Luciferase Reporter Assay Kit (Promega) according to manufacturer's instruction. Reporter activity was measured using a Fluoroskan Ascent FL (Thermo) and data was normalized to an internal Renilla luciferase control. An analogous approach was taken in 293 cells for testing the effects of Msi1 induction and knockdown on the CTTNB1 and NUMB 3'UTRs that were cloned into pmirGLO constructs. Msi1 overexpression was achieved using pCDNA6, and knockdown using and anti-Msi1 shRNA in the pSicoR vector. Luciferase experiments shown are representative of 4 independent experiments.

Western Blots

Cells were lysed in RIPA buffer with protease inhibitors (Roche). After quantification using a BCA protein assay kit (Pierce), 20 μg of total protein was separated by 12% SDS-PAGE under denaturing conditions and transferred to PVDF membranes (GE Healthcare). Membranes were blocked in 5% BSA (Sigma) and then incubated with an anti-Msi1 primary antibody (1:1,000; Abcam), NICD (1:1,000; Abcam), Hes1 (1:1,000; Abcam), APC (1:500; Santa Cruz C-20), p-c-Raf (1:1,00; Cell Signaling), p-AKT (T308) (1:1,000; Cell Signaling), p-AKT (S473) (1:1,000; Cell Signaling), total-AKT (1:1,000; Cell Signaling), p-PDK1 (S241) (1:1,000; Cell Signaling), p-4EBP1 (T37/46) (1:1,000; Cell Signaling), or p-eIF4E (S209) (1:1,000; Cell Signaling), followed by incubation with a secondary antibody conjugated with horseradish peroxidase (HRP) (1:2,000; Cell Signaling) together with an HRP-conjugated primary antibody for β-actin (1:10,000; Sigma). Immunoreactive proteins were visualized using LumiGLO chemiluminescent substrate (Pierce).

Oncomine Analysis

Using Oncomine analysis, Msi1 expression level was analyzed in the Kaiser colon database. The database includes full transcriptome profiles of 105 samples: Control (5); Cecum Adenocarcinoma (17); Colon Adenocarcinoma (41); Colon Mucinous Adenocarcinoma (13); Colon Signet Ring Cell Adenocarcinoma (2); Colon Small Cell Carcinoma (2); Rectal Adenocarinoma (8); Rectal Mucinous Adenocarcinoma (4); Rectal Signet Ring Cell Adenocarcinoma (1); Rectosigmoid Adenocarcinoma (10); Rectosigmoid Mucinous Adenocarcinoma (2)(Rhodes et al., 2007).

PTEN Immunoprecipitation and Activity Assay

Cells (293 & RKO) from 100 mm culture dish at 70-80% were lysed with 0.5 mL of ice cold IP Lysis Buffer (25mM Tris pH 8.0, 150 mM NaCl, 1% NP-40, 1mM EDTA, 5% Glycerol). 400 μL of the cell lysate was Transferred to a fresh, cold, 1.5 mL centrifuge tube. 8 μL of the anti-PTEN antibody (Cell Signaling, #9188) was added to the lysate followed by overnight incubation at 4°C with agitation. 60 μL of the Protein A Dynabeads was added to the mixture and incubated 2-3 hours at 4°C. The bead complex was washed and resuspended in 30 μL of PTEN Reaction buffer. Proceed immediately with the PTEN reactions by adding 30 μL of the 16 μM PI(3,4,5)P3 Substrate to the bead complex. The ELISA was performed following manufacturer's protocol (Echelon, K-4700).

PIP3 Flow Cytometry

Colorectal cancer cell lines were cultured in DMEM+ 10% FBS and transfected with pSicoR vector to knockdown Msi1 and Msi2 using Fugene HD (Promega) according to user manual. EGFP is expressed from pSicoR as a marker to select for transfected cells. Transfected cells were harvested by trypsinization 72 hours post-transfection, washed and resuspended in PBS containing 1 uL/ml of fixable viability dye eFluor 450(Affymetrix ebioscience). Cells were incubated on ice for 30 minutes and were washed two times with PBS. Then, cells were fixed and permeabilized using Cytofix/ Cytoperm solution (BD PharMingen), stained with FITC-anti-GFP (Abcam) and biotinylated anti-PIP3 (Echelon inc.) for 30 min on ice and washed twice. They were incubated with Streptavidin-Allophycocyanin (APC) (biolegend) for 30 min on ice

and washed twice. Flow cytometry was performed on LSRFoirtessa and Flowjo software was used for data analysis.

Crypt Culture

Crypt culture was performed as previously (Sato et al., 2009). After intestinal crypt isolation, a total of 500-1000 crypts were mixed with 50 µl of Matrigel (BD Bioscience) and plated in 24-well plates. After polymerization of Matrigel, 500 µl of crypt culture medium (Advanced DMEM/F12 containing growth factors (50 ng/ml EGF (Invitrogen), 1 µg/ml R-spondin 1 (Wistar Institute protein production facility), 100 ng/ml Noggin (Peprotech) and 3 µM GSK-3 inhibitor (CHIR99021, Stemgent) was added. After 2-day culture at 37 °C incubator, the organoids were treated with 0.2 µg/ml Dox (n=3). 10 organoids were randomly selected from each well and photographed at day 4, day 5, and day 6, and bud length was measured for all buds in each organoid. The error bars represent the standard deviation from three biological replicates.

Xenograft Assays

6-week-old female nude mice were obtained from the Stem Cell and Xenograft Core at UPENN. Stably infected colorectal cancer cells were trypsinized and suspended in phosphate-buffered saline (PBS). A total volume of 0.2 ml containing 2-5 X 10^6 cells and 25% volume MatriGEL was injected subcutaneously into the mouse flank. Tumor size was measured using a Vernier caliper. Tumor volumes were calculated using the formula $V=1/2\ (LxW^2)$, where L is length (longest dimension) and W is width (shortest dimension) of the tumor. Moribund animals were euthanized according to the protocols of the University of Pennsylvania. Tumor growth rates in the xenograft experiment were evaluated by fitting a linear mixed effects model on the $\log_{10}$-transformed tumor volume with days, experiment indicator (Msi shRNA versus control shRNA), and interaction between days and experiment included as independent variables.

Generation and Verification of Msi Floxed Alleles

Msi1 and *Msi2* alleles were targeted using homologous recombination in V6.5 embryonic stem cells. Generation of the *Msi2* conditional allele is described in (Park et al., 2014)Targeted (3-lox) clones were isolated after neomycin (G418) selection and Southern blotting using external probes flanking both the 3' and 5' targeting arm validated proper insertion of the targeting vector. Three-lox clones were then transiently electroporated with Cre recombinase and subcloned to identify 2-lox conditional clones. Clones harboring 2-lox (floxed) Msi1 and Msi2 alleles were injected into blastocysts and resulting chimeras backcrossed to a Black/6 background. Addition of Cre recombinase (either transiently in culture or through intercrossing with *Villin-CreER* mice) resulted in deletion of the transcriptional start site and exons 1&2 (in the case of Msi1) or exons 1-4 (in the case of Msi2), generating a 1-lox null allele that was validated by Southern blotting and Msi protein loss. Southern blotting was carried out by digesting genomic DNA overnight, transferring to Hybond XL membrane (Amersham/GE Healthcare, Pittsburgh, PA) and hybridizing with a ^{32}P-probe labeled by random priming (Prime-it II, Agilent Technologies, Santa Clara CA) in Church buffer at 60°C overnight followed by washing with increasing stringency SDS/SSC buffer and exposure to film.

$Apc^{min/+}$ Tumor Model

The $Apc^{min/+}$ mice were obtained from JAX lab (Stock Number: 002020). $Apc^{min/+}$*::Msi1/2*$^{flox/flox}$ mice with or without the *Villin-CreER* allele (el Marjou et al., 2004) were given 5 doses of

tamoxifen (2mg/dose in 100ul corn oil) when they were 6 weeks old and then raised on a low protein/high fat diet (Research Diets, D12079B) for 6 months. Additional series of tamoxifen doses was given 2 and 4 months post-initiation of high fat diet to maximize recombination of floxed *Msi* alleles. Adenomas were scored by two independent researchers using a stereomicroscope.

Figure 1

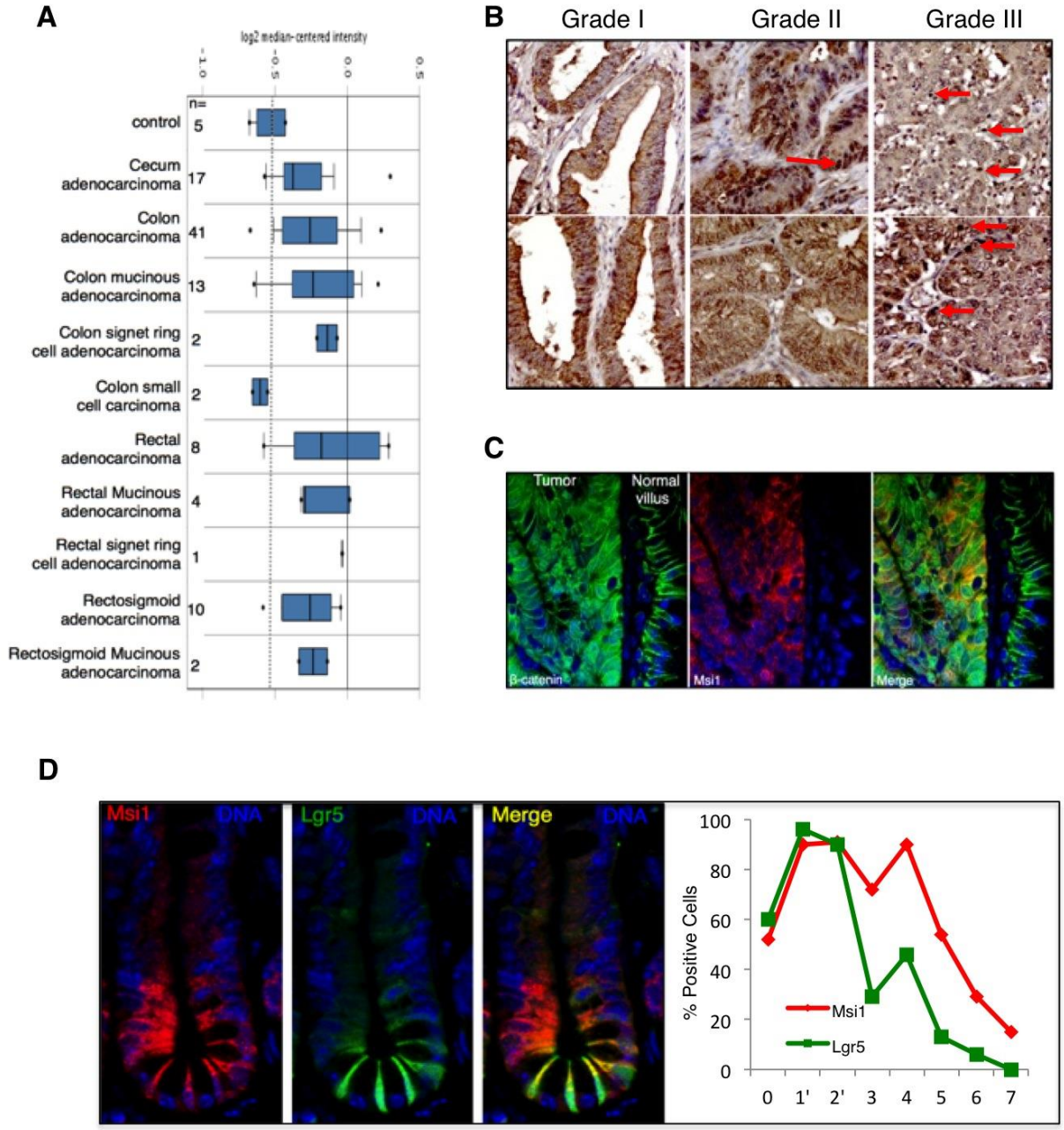
A
log2 median-centered intensity
-1.0
-0.5
0.0
0.5
n=
control 5
Cecum adenocarcinoma 17
Colon adenocarcinoma 41
Colon mucinous adenocarcinoma 13
Colon signet ring cell adenocarcinoma 2
Colon small cell carcinoma 2
Rectal adenocarcinoma 8
Rectal Mucinous adenocarcinoma 4
Rectal signet ring cell adenocarcinoma 1
Rectosigmoid adenocarcinoma 10
Rectosigmoid Mucinous adenocarcinoma 2
B
Grade I
Grade II
Grade III
C
Tumor
Normal villus
β-catenin
Msi1
Merge
D
Msi1
DNA
Lgr5
DNA
Merge
DNA
% Positive Cells
100
80
60
40
20
0
Msi1
Lgr5
0
1'
2'
3
4
5
6
7

Figure 1. Expression of the Msi1 RNA binding protein in intestinal cancers. A. Oncomine transcriptome profiling data demonstrating increased *MSI1* expression in a panel of human gastrointestinal cancers relative to control tissue. The number of samples for each tumor type are indicated. **B**. Immunohistochemical staining for MSI1 in graded human colorectal cancer sections shows strong reactivity in epithelial cells in all grades. Arrows indicate cells with nuclear MSI1 staining (200x magnification). Expression of Msi1 in the intestine from published microarray data after APC deletion (Sansom et al., 2004), after Ctnnb1 deletion (Fevr et al., 2007), after Ck1α deletion (Elyada et al. 2011), and upon dox-induction of non-degradable, activated β-catenin (Hirata et al., 2013). **C.** Immunofluorescence of adenomas resulting from *APC* LOH in the $APC^{min/+}$ mouse showing cytoplasmic and nuclear accumulation of β-catenin and induction of cytoplasmic Msi1 in transformed cells in an adenoma neighboring normal villi, where β-catenin is restricted to adherens junctions at cell membranes and Msi1 is absent (200x magnification). **D.** Immunofluorescence staining of Msi1 (red) in stem cells of the intestinal crypt costained for the crypt base columnar stem cell marker Lgr5 in *Lgr5-eGFP-IRES-CreER* knockin mice (green) (400x magnification). Right panel shows positional quantification of Msi1 and Lgr5 expression in the intestinal crypt, with the cell at the crypt base assigned the 0 position. Paneth cells are not scored.

Figure 2

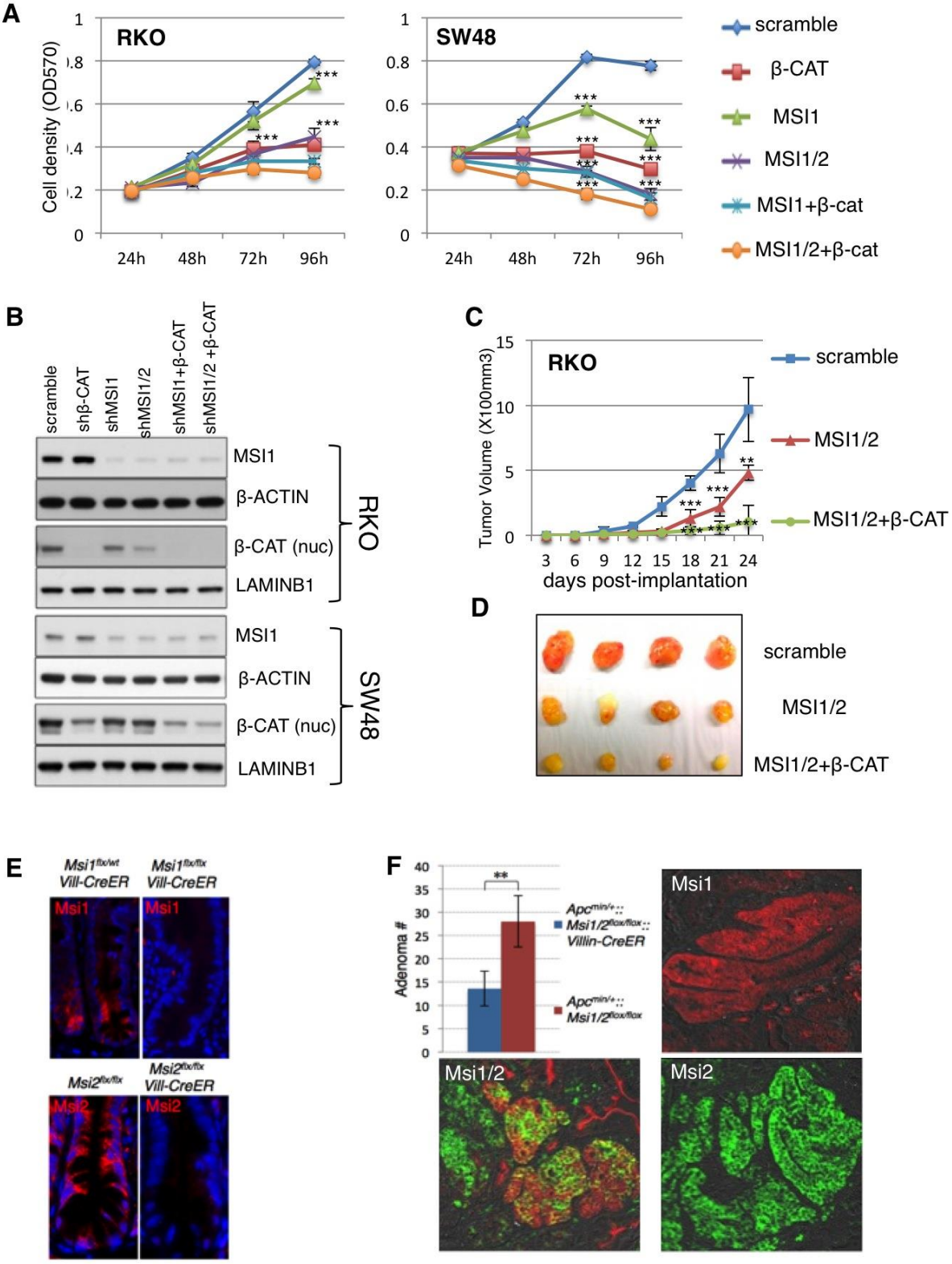
A
RKO
SW48
Cell density (OD570)
24h
48h
72h
96h
scramble
β-CAT
MSI1
MSI1/2
MSI1+β-cat
MSI1/2+β-cat
B
scramble
shβ-CAT
shMSI1
shMSI1/2
shMSI1+β-CAT
shMSI1/2 +β-CAT
MSI1
β-ACTIN
β-CAT (nuc)
LAMINB1
RKO
SW48
C
RKO
Tumor Volume (X100mm3)
days post-implantation
scramble
MSI1/2
MSI1/2+β-CAT
D
scramble
MSI1/2
MSI1/2+β-CAT
E
Msi1flx/wt Vill-CreER
Msi1flx/flx Vill-CreER
Msi1
Msi2flx/flx
Msi2flx/flx Vill-CreER
Msi2
F
Adenoma #
Apcmin/+;; Msi1/2flox/flox;; Villin-CreER
Apcmin/+;; Msi1/2flox/flox
Msi1
Msi1/2
Msi2

Figure 2. Msi activity is required for intestinal tumorigenesis. A. Growth of human colorectal cancer cell lines RKO and SW48 is dramatically inhibited upon shRNA-knockdown of MSI1, MSI1 and MSI2, MSI1 and β-CATENIN. The growth inhibition is most pronounced with dual inhibition of MSI1&2 and β-CATENIN. **B**. Immunoblotting validating knockdown of MSI1 and transcriptionally active (nuclear) β-CATENIN in RKO and SW48 cells. Of note, β-CATENIN knockdown does not affect MSI1 levels, and MSI1 knockdown does not affect nuclear β-CATENIN levels. **C**. Growth of RKO cell xenografts upon MSI1/2 shRNA knockdown or combined MSI1/2 & β-CATENIN knockdown. **D**. Tumors from (**C**) after dissection upon termination of the experiment. **E.** Immunofluorescence staining showing loss of Msi1 and Msi2 proteins from intestinal crypts 5 days after *Villin-CreER*-mediated recombination (mag. 400x). **F**. Growth of adenomas in $APC^{min/+}$ mice with or without deletion of *Msi* gene deletion in $Msi1/2^{flox/flox}$*::Villin-CreER::*$APC^{min/+}$ mice (n=5-6). Representative immunofluorescence micrographs of residual tumors in $Msi1/2^{flox/flox}$*::Villin-CreER::*$APC^{min/+}$ mice showing Msi1 (red), Msi2 (green), or Msi1/2 expression (100%, 68 of 68 total residual tumors scored positive). Magnification 200x. **: $p< 0.005$, ***: $p< 0.0005$. See also **Figure S1**.

Figure 3

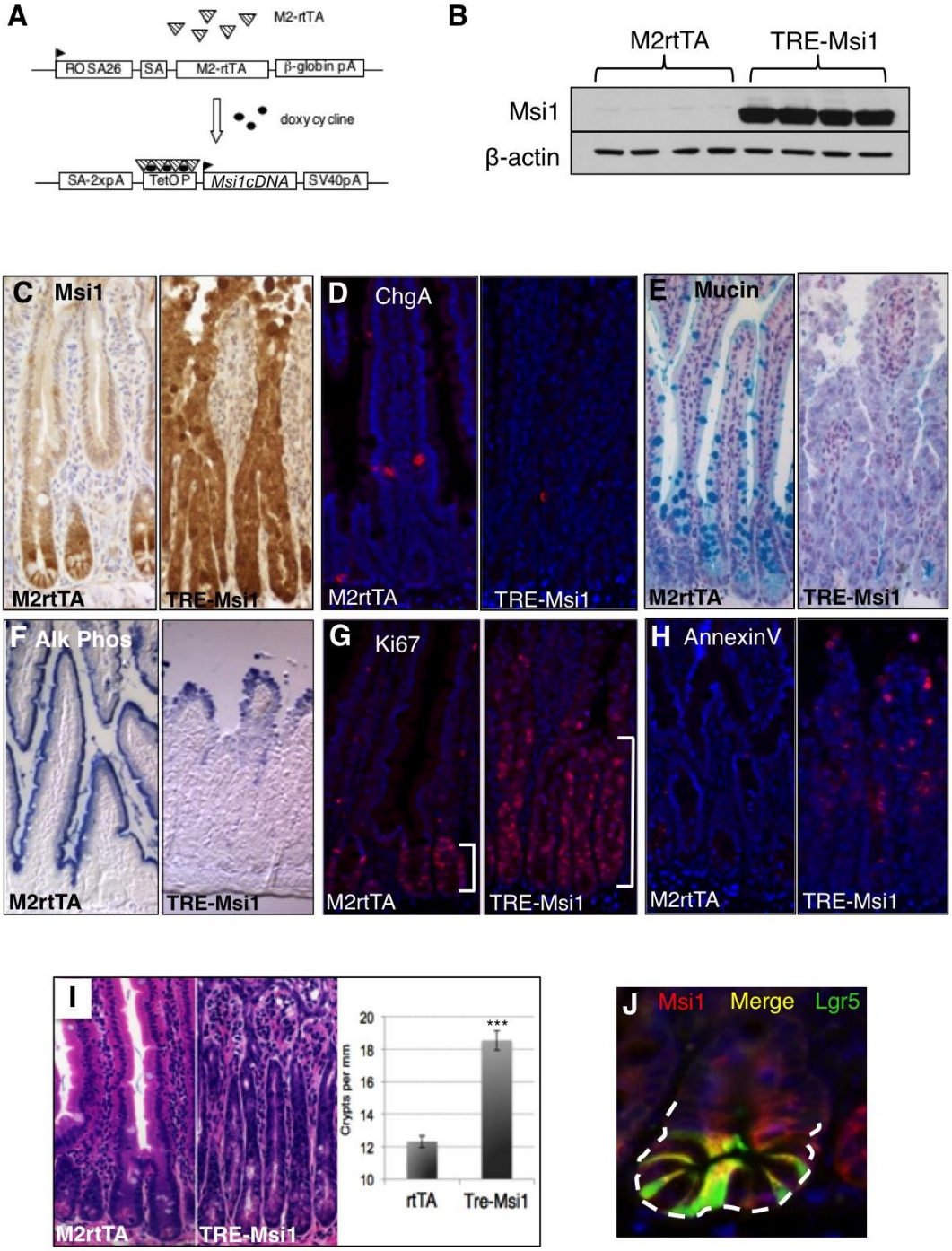
A
M2-rtTA
ROSA26
SA
M2-rtTA
β-globin pA
doxycycline
SA-2xpA
TetOP
Msi1cDNA
SV40pA
B
M2rtTA
TRE-Msi1
Msi1
β-actin
C Msi1
M2rtTA
TRE-Msi1
D ChgA
M2rtTA
TRE-Msi1
E Mucin
M2rtTA
TRE-Msi1
F Alk Phos
M2rtTA
TRE-Msi1
G Ki67
M2rtTA
TRE-Msi1
H AnnexinV
M2rtTA
TRE-Msi1
I
M2rtTA
TRE-Msi1
Crypts per mm
20
18
16
14
12
10
***
rtTA
Tre-Msi1
J Msi1 Merge Lgr5

Figure 3. Constitutive expression of the intestinal stem cell-specific RNA binding protein Msi1 blocks differentiation and drives proliferation. A. Design of doxycycline (Dox)-inducible *Msi1* knockin mice harboring a modified reverse tetracycline transactivator (*M2rtTA*) at the *ROSA26* locus and the *Msi1* cDNA under control of the tetracycline-responsive element (*TRE/TetOP*) targeted downstream of the *Col1a1* locus (upper panel)**. B.** Administration of Dox to the drinking water of a cohort of 4 control (*M2rtTA*) and 4 *Msi1*-inducible (*TRE-Msi1*) transgenic mice for 24 hours results in strong, consistent induction of Msi1 expression in purified intestinal epithelium detected by immunoblotting (lower panel). **C-H.** Representative immunohistochemistry for Msi1 (**C**), immunofluorescence for enteroendocrine marker Chromogranin-A (**D**), Alcian blue staining of goblet cell mucin (**E**), alkaline phosphatase staining of enterocyte activity (**F**), immunofluorescence staining for Ki-67 marking proliferative cells (**G**), and immunofluorescence staining for apoptotic cells with annexin-V (**H**) in control (*M2rtTA*) and *TRE-Msi1* intestinal epithelium 48hrs after Dox treatment. Brackets in (**G**) indicate the height of the crypt proliferative zone. **I**. Histological sections showing extension of crypt height and increased crypt fission in *TRE-Msi1* mice (quantified at right, n=3) (***: $p<0.0005$). **J.** A crypt undergoing fission in *Lgr5-eGFP-IRES-CreER* knockin mice costained for Msi1 (red) and *Lgr5-eGFP* (green) at the site of fission. **C-I**; 200x magnification, **J**; 400x magnification. Also see **Figure S2.**

Figure 4

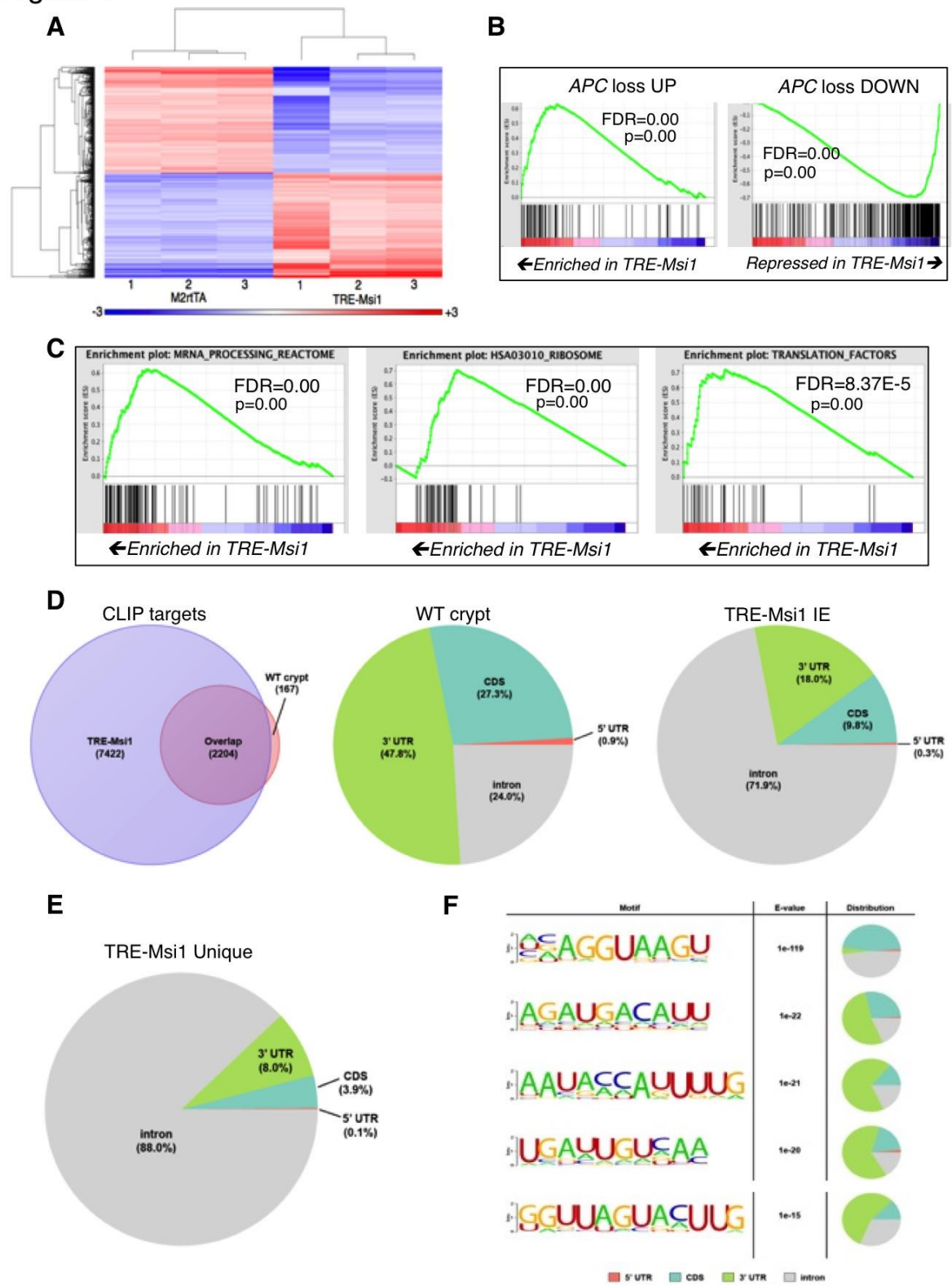
A
1
2
3
M2rtTA
1
2
3
TRE-Msi1
-3
+3
B
APC loss UP
FDR=0.00
p=0.00
APC loss DOWN
FDR=0.00
p=0.00
Enriched in TRE-Msi1
Repressed in TRE-Msi1
C
Enrichment plot: MRNA_PROCESSING_REACTOME
FDR=0.00
p=0.00
Enrichment plot: HSA03010_RIBOSOME
FDR=0.00
p=0.00
Enrichment plot: TRANSLATION_FACTORS
FDR=8.37E-5
p=0.00
Enriched in TRE-Msi1
Enriched in TRE-Msi1
Enriched in TRE-Msi1
D
CLIP targets
TRE-Msi1 (7422)
Overlap (2204)
WT crypt (167)
WT crypt
CDS (27.3%)
5' UTR (0.9%)
3' UTR (47.8%)
intron (24.0%)
TRE-Msi1 IE
3' UTR (18.0%)
CDS (9.8%)
5' UTR (0.3%)
intron (71.9%)
E
TRE-Msi1 Unique
3' UTR (8.0%)
CDS (3.9%)
5' UTR (0.1%)
intron (88.0%)
F
Motif
E-value
Distribution
1e-119
1e-22
1e-21
1e-20
1e-15
5' UTR
CDS
3' UTR
intron

Figure 4. Global transcriptome profiling and RNA binding analysis of Msi1. A. Heatmap and hierarchical clustering of transcriptome profiles performed on 3 control *(M2rtTA)* and 3 *TRE-Msi1* mice treated with Dox for 24 hours. **B.** Gene Set Enrichment Analysis (GSEA) of the *TRE-Msi1* transcriptome 24 hours after Dox induction identifies activation of genes induced by acute *APC* deletion in the intestinal epithelium (*APC* loss up) and suppression of genes downregulated after *APC* deletion (*APC* loss down). **C.** GSEA plots showing an enrichment in mRNA processing, splicing, ribosomal and translation components upon Msi1 induction. **D**. Venn diagram showing overlap between Msi1-bound transcripts in wildtype crypts and *TRE-Msi1* intestinal epithelium 24 hours after Dox induction (left) and the distribution of Msi1 RNA binding events in wildtype crypts and *TRE-Msi1* epithelium (center, right). **E**. Distribution of binding events in the 7422 transcripts Msi1 unique to *TRE-Msi1* induced epithelium versus wildtype crypts. **F**. Msi1 binding motif identification and distribution in wildtype intestinal crypts. The fifth motif represents the motif previously identified by selex *in vitro*. FDR=false discovery rate. Also see **Figure S3**.

Figure 5

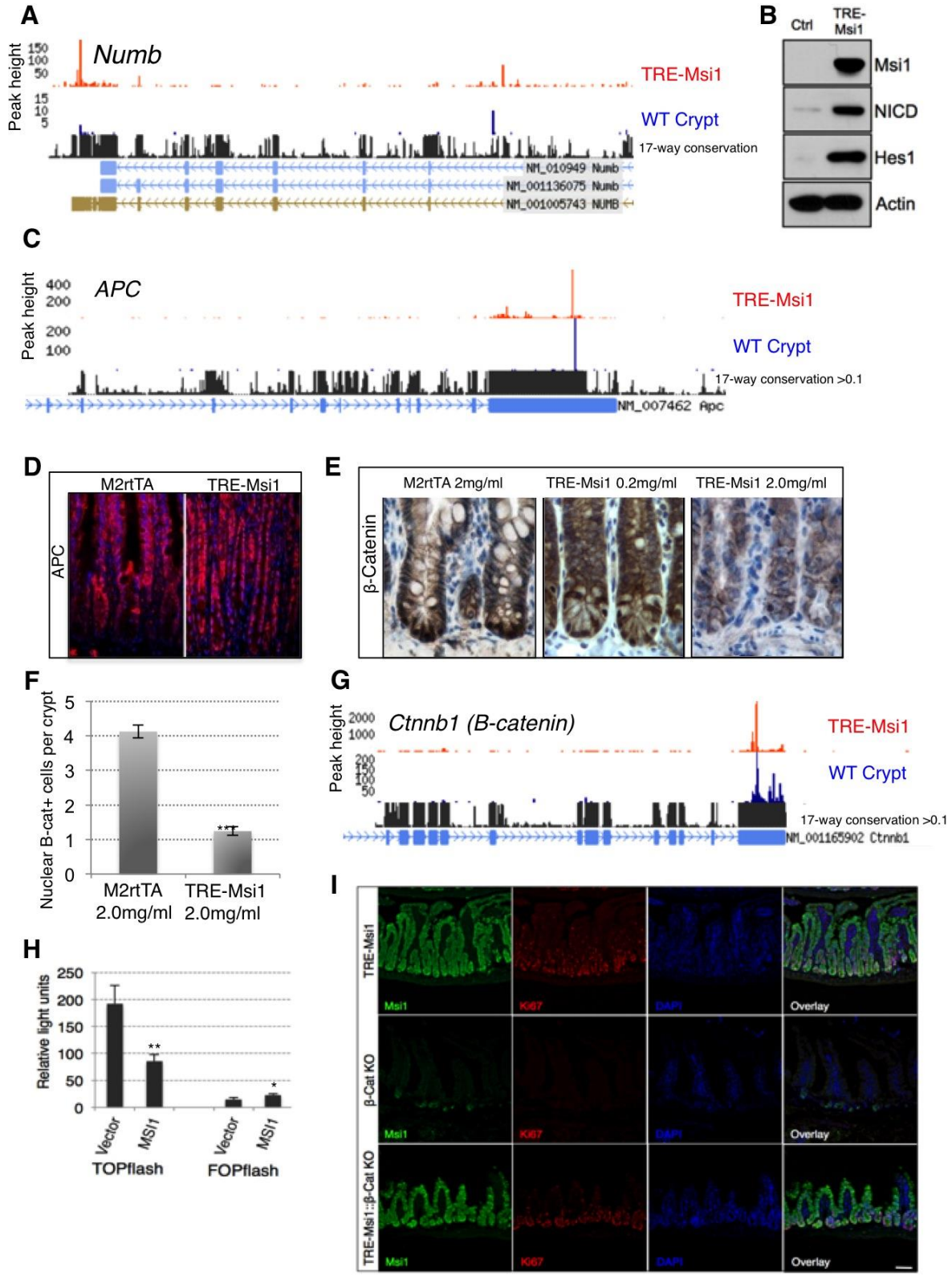
A
Numb
Peak height
TRE-Msi1
WT Crypt
17-way conservation
NM_010949 Numb
NM_001136075 Numb
NM_001005743 NUMB
B
Ctrl
TRE-Msi1
Msi1
NICD
Hes1
Actin
C
APC
Peak height
TRE-Msi1
WT Crypt
17-way conservation >0.1
NM_007462 Apc
D
M2rtTA
TRE-Msi1
APC
E
M2rtTA 2mg/ml
TRE-Msi1 0.2mg/ml
TRE-Msi1 2.0mg/ml
β-Catenin
F
Nuclear B-cat+ cells per crypt
M2rtTA 2.0mg/ml
TRE-Msi1 2.0mg/ml
G
Ctnnb1 (B-catenin)
Peak height
TRE-Msi1
WT Crypt
17-way conservation >0.1
NM_001165902 Ctnnb1
H
Relative light units
Vector
MSI1
TOPflash
FOPflash
I
TRE-Msi1
β-Cat KO
TRE-Msi1::β-Cat KO
Msi1
Ki67
DAPI
Overlay

Figure 5. Effects of Msi1 RNA binding activity on Notch and Wnt pathway activity. A. CLIP-Seq track showing Msi1 binding to the *Numb* 3'UTR, with wildtype Msi1 binding in blue and *Tre-Msi1* binding in red. **B.** Immunoblot analysis demonstrating an activation of the Notch pathway upon *TRE-Msi1* induction via increased presence of the Notch intracellular domain (NICD) and subsequent upregulation of the downstream Notch target gene *Hes1*. **C**. CLIP-Seq track showing Msi1 binding to the *APC* 3'UTR in wildtype crypts and *TRE-Msi1* epithelium. **D.** Immunofluorescence staining of APC protein in control (*M2rtTA*) and *TRE-Msi1* mice 48 hours after dox administration (200x). **E.** Immunohistochemical staining for transcriptionally active (nuclear) β-catenin in crypts of control (*M2rtTA*) and *TRE-Msi1* transformed intestine, at low (0.2 mg/ml) and high (2.0 mg/ml) doxycycline concentrations (400x). **F**. Quantification of β-catenin-positive nuclei in control (*M2rtTA*) and *TRE-Msi1* crypts treated with 2.0mg/ml doxycycline (***: $p<0.0005$). **G**. CLIP-Seq track showing Msi1 binding to the *Ctnnb1* 3'UTR. **H**. Luciferase reporter assays in HCT116 cells for canonical Wnt pathway activation using the TOPflash reporter with multimerized β-catenin/TCF binding sites upstream of luciferase or the control FOPflash reporter with mutated binding sites and empty vector or MSI1 overexpression, light units relative to a constitutive internal Renilla luciferase control (n=3) (*: $p<0.05$, **: $p<0.005$). **I**. Immunofluorescence staining for Msi1 and Ki67 in *TRE-Msi1*, *Ctnnb1* (β-catenin) knockout, and *TRE-Msi1:: Ctnnb1* knockout intestinal epithelium (100x, bar=50um). Also see **Figure S4**.

Figure 6

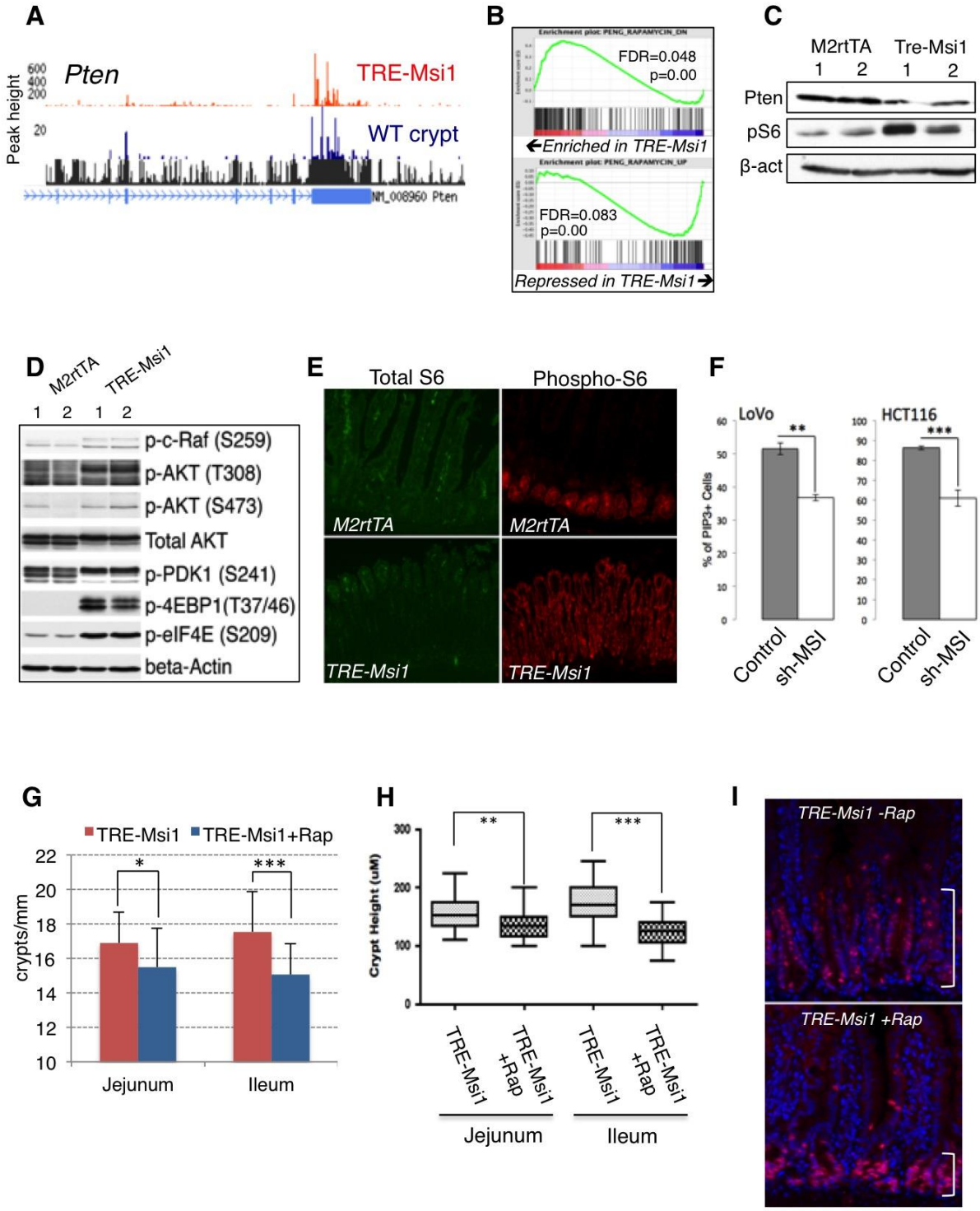
A
Pten
TRE-Msi1
WT crypt
Peak height
600
400
200
20
NM_008960 Pten
B
FDR=0.048
p=0.00
←Enriched in TRE-Msi1
FDR=0.083
p=0.00
Repressed in TRE-Msi1→
C
M2rtTA
Tre-Msi1
1 2 1 2
Pten
pS6
β-act
D
M2rtTA
TRE-Msi1
1 2 1 2
p-c-Raf (S259)
p-AKT (T308)
p-AKT (S473)
Total AKT
p-PDK1 (S241)
p-4EBP1(T37/46)
p-eIF4E (S209)
beta-Actin
E
Total S6
Phospho-S6
M2rtTA
M2rtTA
TRE-Msi1
TRE-Msi1
F
LoVo
HCT116
% of PIP3+ Cells
**
***
Control
sh-MSI
Control
sh-MSI
G
TRE-Msi1
TRE-Msi1+Rap
crypts/mm
*
***
Jejunum
Ileum
H
Crypt Height (uM)
**
***
TRE-Msi1
TRE-Msi1 +Rap
TRE-Msi1
TRE-Msi1 +Rap
Jejunum
Ileum
I
TRE-Msi1 -Rap
TRE-Msi1 +Rap

Figure 6. Activation of the PI3K-AKT-mTORC1 axis downstream of Msi1. A. CLIP-Seq track showing Msi1 binding to the 3'UTR of the Pten tumor suppressor in wild-type crypts (blue) and *TRE-Msi1* epithelium (red). Y-axis indicates peak height in number of sequencing reads. **B**. GSEA plots showing and enrichment of genes suppressed by Rapamycin treatment in *TRE-Msi1* epithelium (top panel) and a suppression of genes induced by Rapamycin treatment (lower panel). **C**. Immunoblotting demonstrates reduction in Pten protein levels concomitant to S6 phosphorylation upon Msi1 induction in the intestinal epithelium. **D**. Immunoblot analysis of the PI3K-AKT-mTORC1 pathway downstream of Pten in the intestinal epithelium of two control and two *TRE-Msi1* mice treated with Dox for 24 hours. **E.** Immunofluorescence showing increased phosphorylation of S6 by the mTORC1 target S6 kinase in control and *TRE-Msi1* transformed intestinal epithelium (100x magnification). **F**. Quantification of PIP3+ cells by flow cytometric analysis in LoVo and HCT116 cells upon MSI1/2 knockdown**. G-H**. Rapamycin treatment rescues *TRE-Msi1*-induced transformation of the intestinal epithelium. Mice treated with Rapamycin for 3 days prior to Dox administration exhibit decreased crypt fission (**G**) and a block in crypt height expansion (**H**) (n=3)(*: $p< 0.05$, **: $p< 0.005$, ***: $p< 0.0005$).
I. Immunofluorescence staining for Ki67 in the proximal jejunum of Dox-induced *TRE-Msi1* mice with or without Rapamycin treatment demonstrates a restriction of the proliferative zone to the crypt after Rap treatment (200x magnification). Also see **Figure S5**.

Figure 7

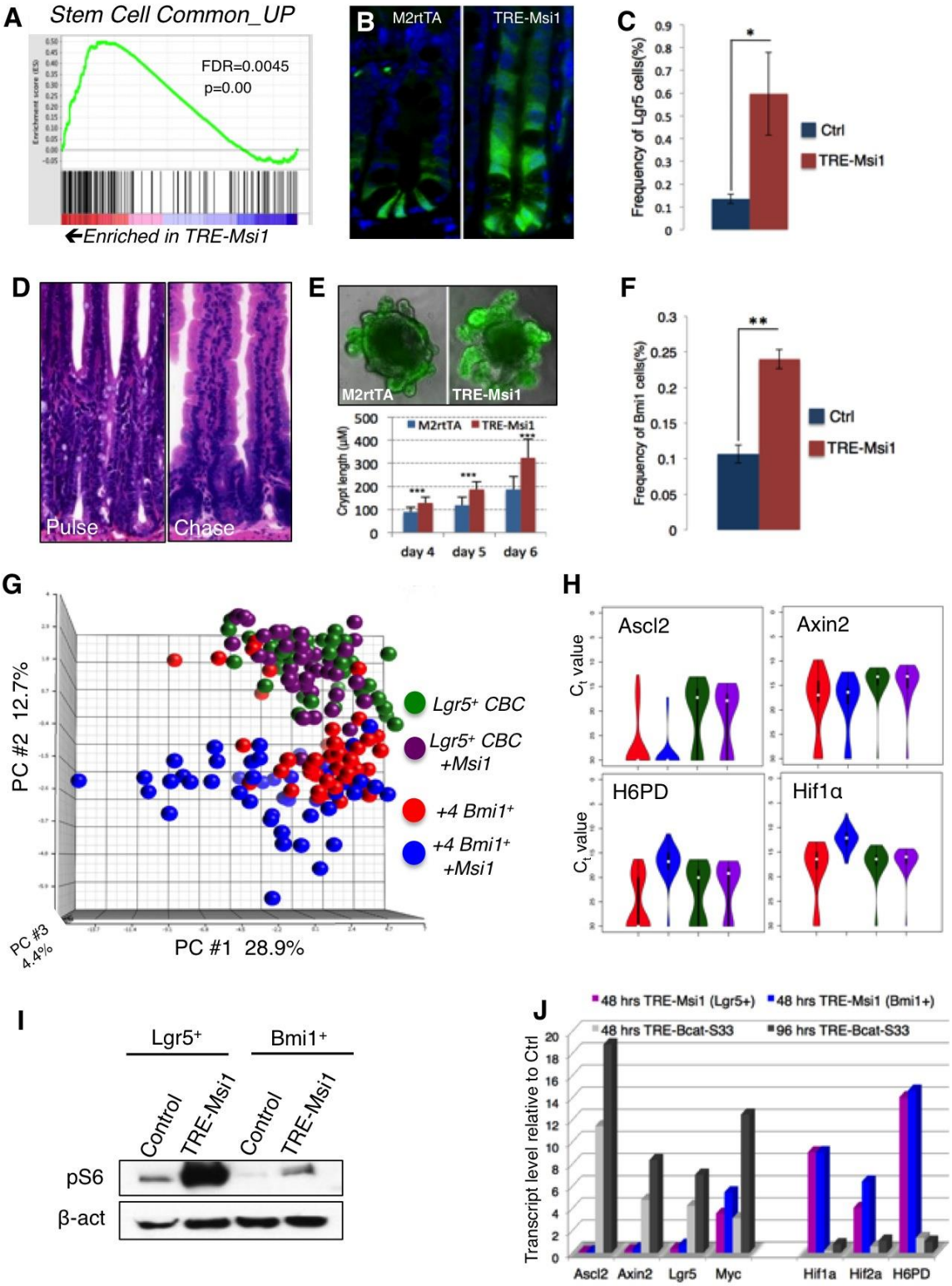
A
Stem Cell Common_UP
FDR=0.0045
p=0.00
Enriched in TRE-Msi1
B
M2rtTA
TRE-Msi1
C
Frequency of Lgr5 cells(%)
Ctrl
TRE-Msi1
D
Pulse
Chase
E
M2rtTA
TRE-Msi1
Crypt length (μM)
day 4
day 5
day 6
F
Frequency of Bmi1 cells(%)
Ctrl
TRE-Msi1
G
PC #2 12.7%
PC #1 28.9%
PC #3 4.4%
Lgr5+ CBC
Lgr5+ CBC +Msi1
+4 Bmi1+
+4 Bmi1+ +Msi1
H
Ascl2
Axin2
H6PD
Hif1α
CT value
I
Lgr5+
Bmi1+
Control
TRE-Msi1
Control
TRE-Msi1
pS6
β-act
J
48 hrs TRE-Msi1 (Lgr5+)
48 hrs TRE-Msi1 (Bmi1+)
48 hrs TRE-Bcat-S33
96 hrs TRE-Bcat-S33
Transcript level relative to Ctrl
Ascl2
Axin2
Lgr5
Myc
Hif1a
Hif2a
H6PD

Figure 7. Msi1 drives activation of the reserve intestinal stem cell population. **A**. GSEA plot showing an enrichment of the *stem cell common up* signature that represents genes commonly expressed across several purified stem cell types (Ramalho-Santos et al., 2002). **B**. The *Lgr5-eGFP*$^+$ zone is expanded upon *TRE-Msi1* induction (mag.=400x). **C**. Treatment of *Lgr5-eGFP::M2rtTA* or *Lgr5-eGFP::TRE-Msi1* with Dox for 48 hours followed by flow cytometric analysis for eGFP+ cells demonstrates a marked increase in response to Msi1 induction (*: $p< 0.05$). **D**. A 48 hour Dox pulse of *TRE-Msi1* mice followed by 4 months chase reveals a reversion to normal crypt-villus architecture (n=3) (mag.=200x). **E**. Crypts purified from *Lgr5-eGFP::M2rtTA* or *Lgr5-eGFP::TRE-Msi1* mice grown in organoid cultures with Dox, with changes in crypt length quantified (n=3) (***: $p< 0.0005$) (mag.=100x). **F.** Flow cytometric analysis of *Bmi1-Tomato*$^+$ cells demonstrates a marked increase in response to 48 hours of Msi1 induction (**: $p< 0.005$). **G.** Principal component analysis of cellular identity in single active crypt base columnar (Lgr5+) stem cells and reserve +4 (Bmi1+) intestinal stem cells with and without Msi1 induction based on the expression profiling of 48 transcripts representing the Wnt pathway, Notch pathway, proliferation, metabolism, and stem cell identity. Each sphere represents a single cell, and the percent of variation ascribed to each of the principle components is delineated on the axes. **H**. Violin plots showing the expression level in the populations of single intestinal stem cells in (**F**). The white dot in the violin plot represents the median expression within the group of cells, the black box represents the interquartile range, and the width of the plot is directly correlated to the number of cells at any given expression level. **I.** Immunoblotting for S6 phosphorylation using equal numbers of sorted Lgr5+ and Bmi1+ ISCs 36hrs after Msi1 induction. **J.** QRT-PCR analysis on equal numbers of sorted reserve +4 stem cells (Bmi1+) and CBCs (Lgr5+) in response to 48 hours of Msi1 induction and purified intestinal crypts in response to activated β-catenin induction (βcat-S33) at the indicated times post-induction. Values represent fold change relative to control (*M2rtTA*+dox). Also see **Figure S6**.

Supplemental Figure 1

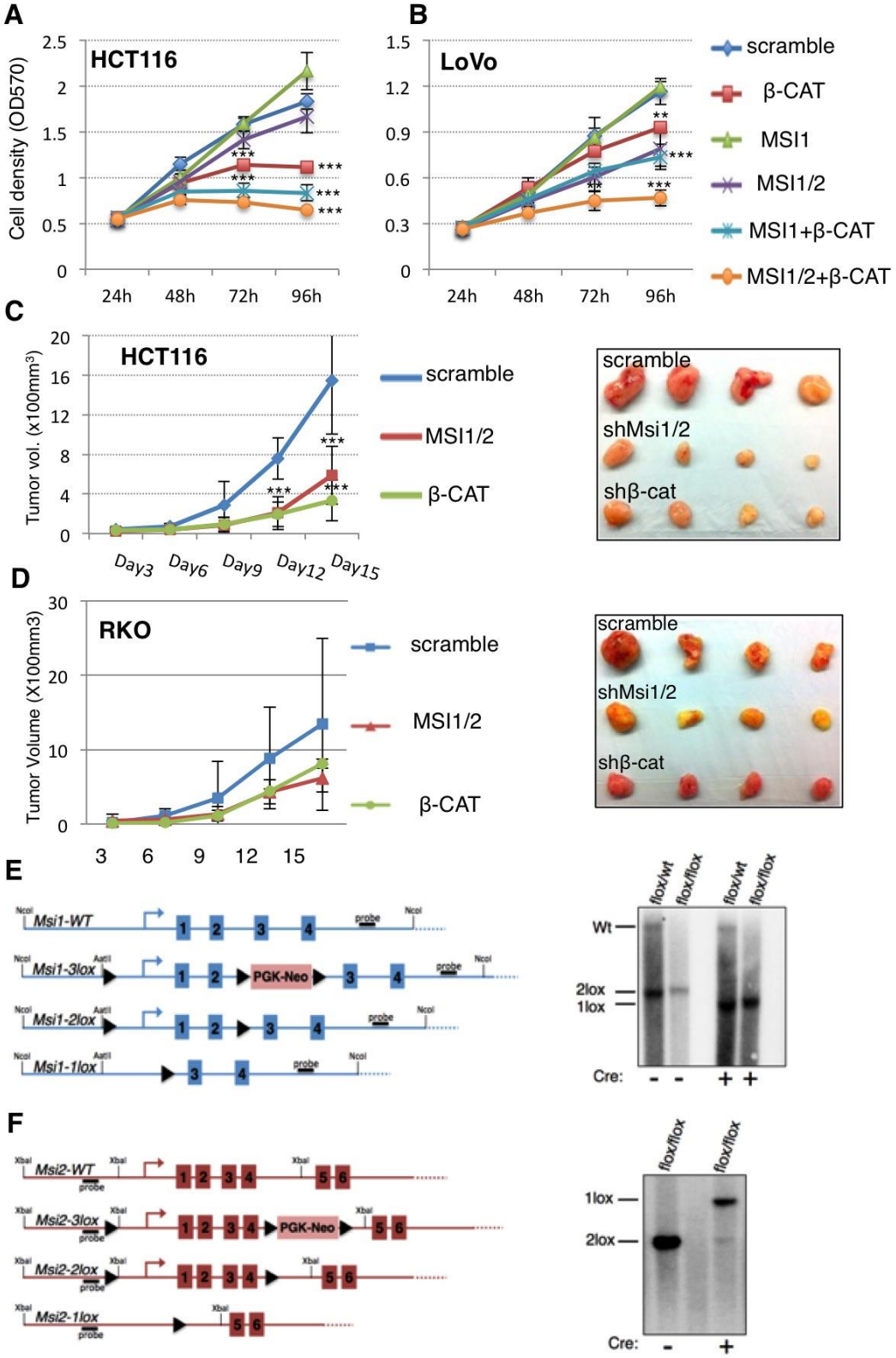

Figure S1. Generation and validation of Msi1 and Msi2 conditional knockout alleles. A-B. Cell proliferation (MTT) assays in HCT116 (**A**) and LoVo (**B**) human colorectal cancer cell lines after lentiviral shRNA knockdown of β-CATENIN, MSI1, MSI1 + MSI2, MSI1 + β-CATENIN, and MSI1 + MSI2 + β-CATENIN versus scrambled shRNA control. **C-D.** Xenograft assays of HCT116 (**C**) and RKO (**D**) cells infected with lentiviral shRNA constructs as indicated followed by monitoring of tumor growth (left) and final tumor size (right). **E-F.** Targeting strategy showing the *3-l*ox alleles after homologous recombination in ES cells, the *2-lox (floxed)* alleles used to generate mouse strains after transient Cre introduction to excise the *PGK-Neo* cassette in culture, and the *1-lox*, null allele generated after Cre recombinase activity from the *Villin-CreER* transgene *in vivo*. Validation of *Villin-CreER* deletion of *Msi1* and *Msi2* by Southern blotting (right) after digestion of genomic DNA with XbaI using an external 5' probe depicted at left. Refers to main **Figure 2.**

Supplemental Figure 2

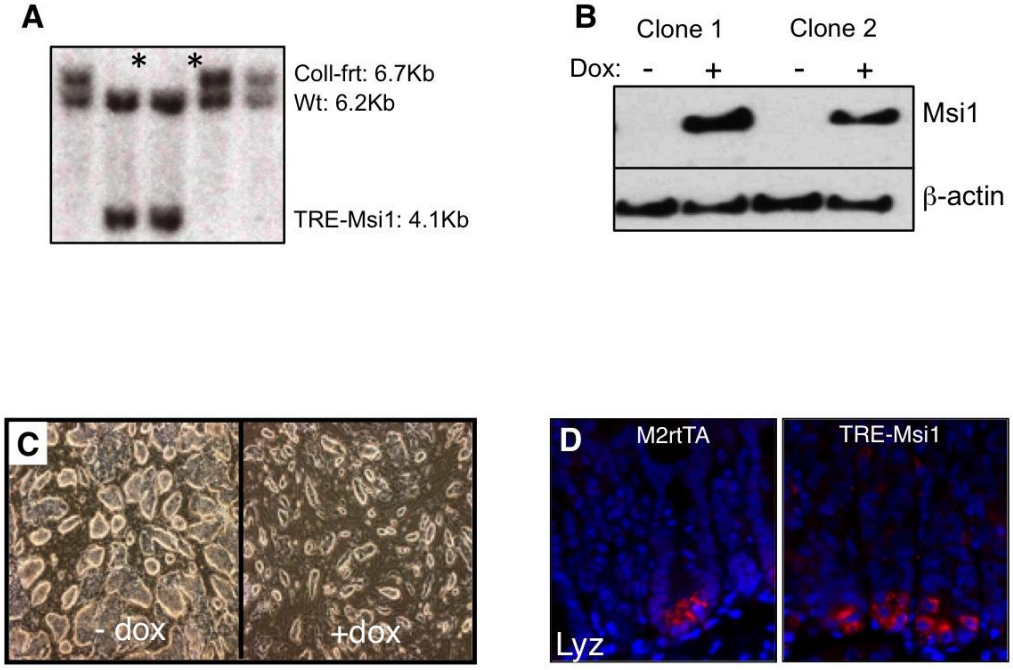

Figure S2. A. Southern blot demonstrating correct flip-in targeting (asterisk) of the *TRE-Msi1* allele downstream of the *Coll1a1* locus. **B.** Induction of the *TRE-Msi1* allele in targeted ES cell clones shown by immunoblot. **C.** Effects of *TRE-Msi1* induction in targeted ES cells from **(B)**. **D.** Immunofluorescence detecting Paneth cells at the crypt base via Lysozyme staining in control (*M2rtTA*) and *TRE-Msi1* mice treated with Dox for 48 hours (mag. 400x) Refers to main **Figure 3**.

Supplemental Figure 3

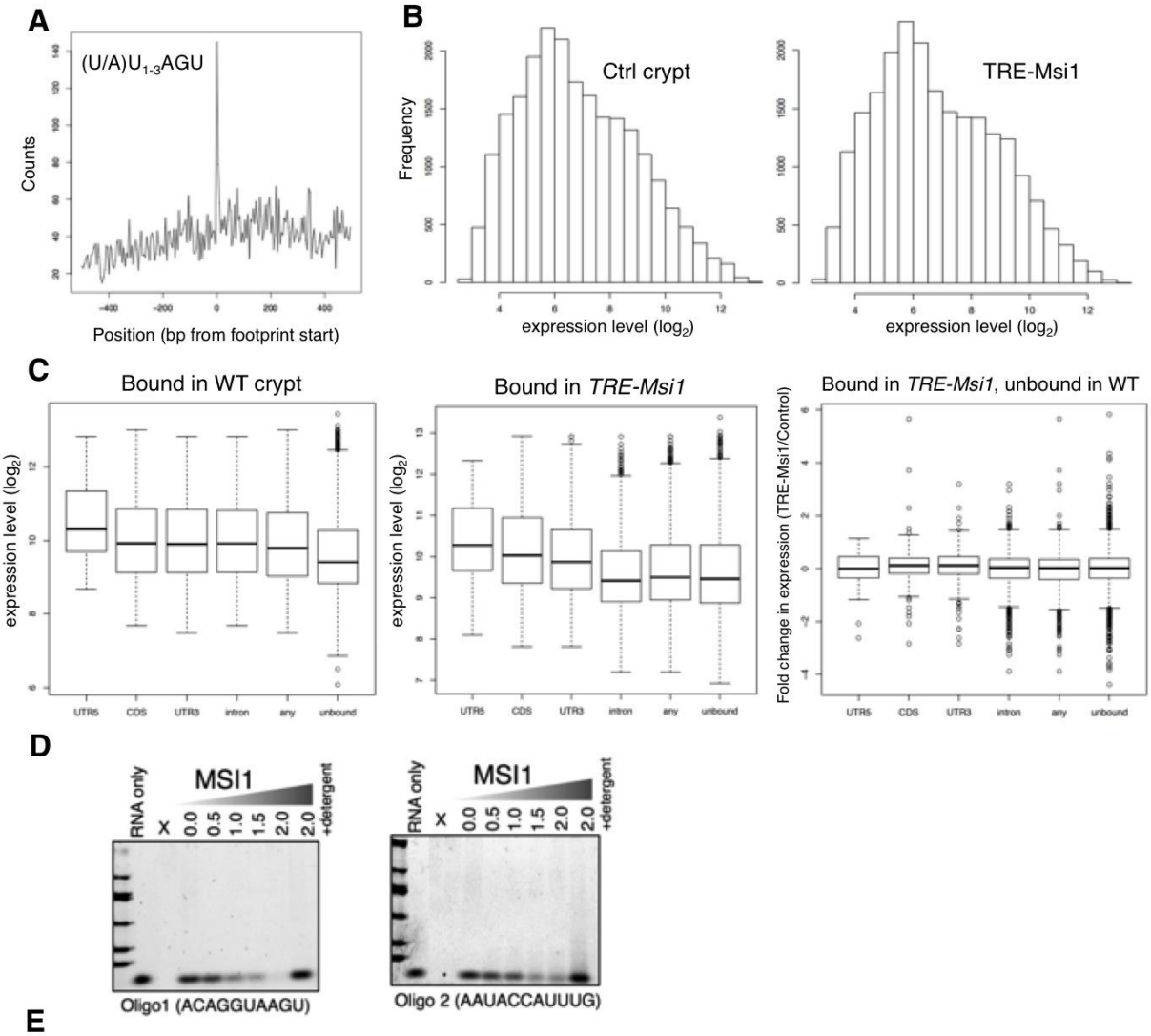

E

WT Crypt: All targets		WT Crypt: 3'UTR targets		TRE-Msi1 IE: 3'UTR targets	
GO Term	*P-Value*	*GO Term*	*P-Value*		*P-Value*
protein localization	5.20E-19	protein transport	3.50E-19	protein transport	8.30E-26
protein transport	6.50E-19	establishment of protein localization	6.90E-19	establishment of protein localization	2.40E-25
establishment of protein localization	1.40E-18	protein localization	4.20E-18	protein localization	1.80E-23
nucleotide binding	1.30E-15	intracellular transport	3.80E-12	intracellular transport	3.10E-18
intracellular transport	4.80E-14	cellular macromolecule localization	7.10E-11	cellular macromolecule localization	2.40E-16
cellular macromolecule localization	8.40E-13	intracellular protein transport	1.10E-10	cellular protein localization	3.40E-16
cellular protein localization	1.60E-12	cellular protein localization	1.50E-10	intracellular protein transport	2.10E-15
purine nucleotide binding	4.20E-10	nucleotide binding	1.80E-09	nucleotide binding	5.40E-15
ribonucleotide binding	7.00E-09	purine nucleotide binding	1.80E-05	RNA binding	1.90E-12
purine ribonucleotide binding	7.00E-09	unfolded protein binding	3.10E-05	cofactor binding	1.50E-07
RNA binding	7.90E-09	RNA binding	3.60E-05	purine nucleotide binding	3.80E-07
purine nucleoside binding	6.30E-08	ribonucleotide binding	2.30E-04	ribonucleotide binding	3.50E-06
nucleoside binding	7.60E-08	purine ribonucleotide binding	2.30E-04	mRNA binding	5.50E-05
KEGG Pathway	*P-Value*	*KEGG Pathway*	*P-Value*	*KEGG Pathway*	*P-Value*
Adherens junction	7.20E-07	Adherens junction	3.00E-06	Adherens junction	2.60E-08
Citrate cycle (TCA cycle)	1.50E-05	Citrate cycle (TCA cycle)	3.50E-06	Tight junction	1.10E-06
Wnt signaling pathway	1.80E-05	N-Glycan biosynthesis	1.00E-04	Citrate cycle (TCA cycle)	7.20E-06
Ribosome	2.20E-05	Tight junction	2.00E-05	Pathways in cancer	6.90E-05
Tight junction	1.40E-04	Wnt signaling pathway	1.60E-03	Wnt signaling pathway	1.60E-03

Figure S3. A. Position of the canonical Msi1 recognition motif previously identified *in vitro* within CLIP-Seq reads containing that motif. **B.** Expression levels of Msi1 CLIP targets plotted against the frequency of binding events in wildtype crypts and *TRE-Msi1* epithelium. **C.** Expression levels of Msi1 CLIP targets of various classes, including those newly bound after *TRE-Msi1* activation relative to wildtype crypts (right panel, Y-axis represents the fold change in expression in *TRE-Msi1* epithelium relative to control). **D.** Msi1 RNA binding assays demonstrating dose-dependent interaction between Msi1 and consensus motif oligos derived from CLIP studies (shown in **Figure 4F**). **E.** Gene ontology (GO) and KEGG pathway analysis of all Msi1 RNA binding targets in wildtype crypts (left), 3'UTR binding targets in wildtype crypts (center), and 3'UTR targets in *TRE-Msi1* epithelium (right) after 24 hours of Dox administration. Refers to main **Figure 4**.

Supplemental Figure 4

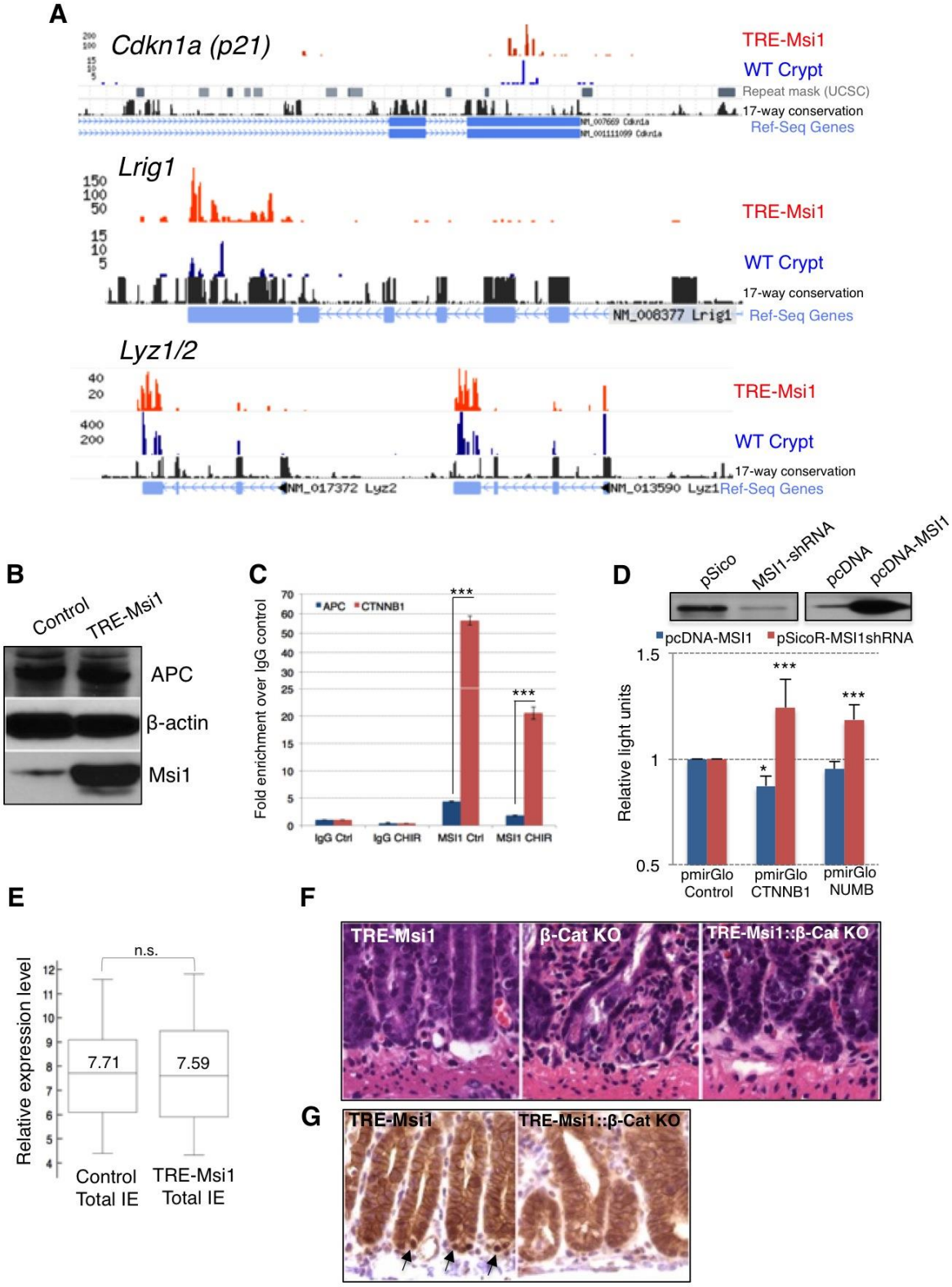

Figure S4. A. CLIP-Seq tracks of Msi1 bound to the *Cdkn1a*, *Lrig1*, *Lyz1* and *Lyz2* transcripts in wildtype crypts and *TRE-Msi1* epithelium. Y-axes indicate peak height in number of sequence tags. Binding of ectopic Msi1 in *TRE-Msi1* epithelium is shown in red, binding of endogenous Msi1 in wildtype crypts is shown in blue. **B.** Immunoblotting for APC in the epithelium of TRE-Msi1 and control mice. **C.** CLIP-qRT-PCR analysis of endogenous MSI1 binding to 3'UTRs of *APC* and *CTNNB1* in HEK293 cells in the absence (Ctrl) or presence of GSK3β inhibitor CHIR99021 (CHIR) (n=3)(*** : $p< 0.0005$). Y-axis plotted as fold enrichment over IgG control IP. **D.** Luciferase reporter assays in 293T cells upon lentiviral shRNA-knockdown of MSI1 (using pSico) or MSI1 overexpression (using pcDNA), validated by Western blotting (top). Luciferase assays (bottom) shown for constructs containing the CTNNB1 and NUMB 3'UTRs (n=3) (*: $p<0.05$, ***: $p< 0.0005$). Y-axis plotted as light units from Firefly luciferase in reporter constructs relative to internal Renilla luciferase control. **E.** Box plot showing expression levels of known direct β-catenin target genes (full gene list in methods) in total intestinal epithelium from control (*M2rtTA*) and *TRE-Msi1* mice (n=3). **F.** Loss of crypt epithelial architecture upon genetic ablation of *Ctnnb1*, comparing *TRE-Msi1* mice (left), *Ctnnb1*$^{flox/flox}$*::VillinCreERT2* mice (center), and *TRE-Msi1:: Ctnnb1*$^{flox/flox}$*::VillinCreERT2* (right), 48 hours after Msi1 induction and a total of 5 days after *Ctnnb1* deletion (400x) **G.** Immunostaining for transcriptionally active (nuclear) β-catenin in TRE-Msi1 epithelium (left, arrows) and *TRE-Msi1:: Ctnnb1*$^{flox/flox}$*::VillinCreERT2* epithelium (right) where there is a complete absence of nuclear β-catenin (400x). Refers to main **Figure 5**.

Supplemental Figure 5

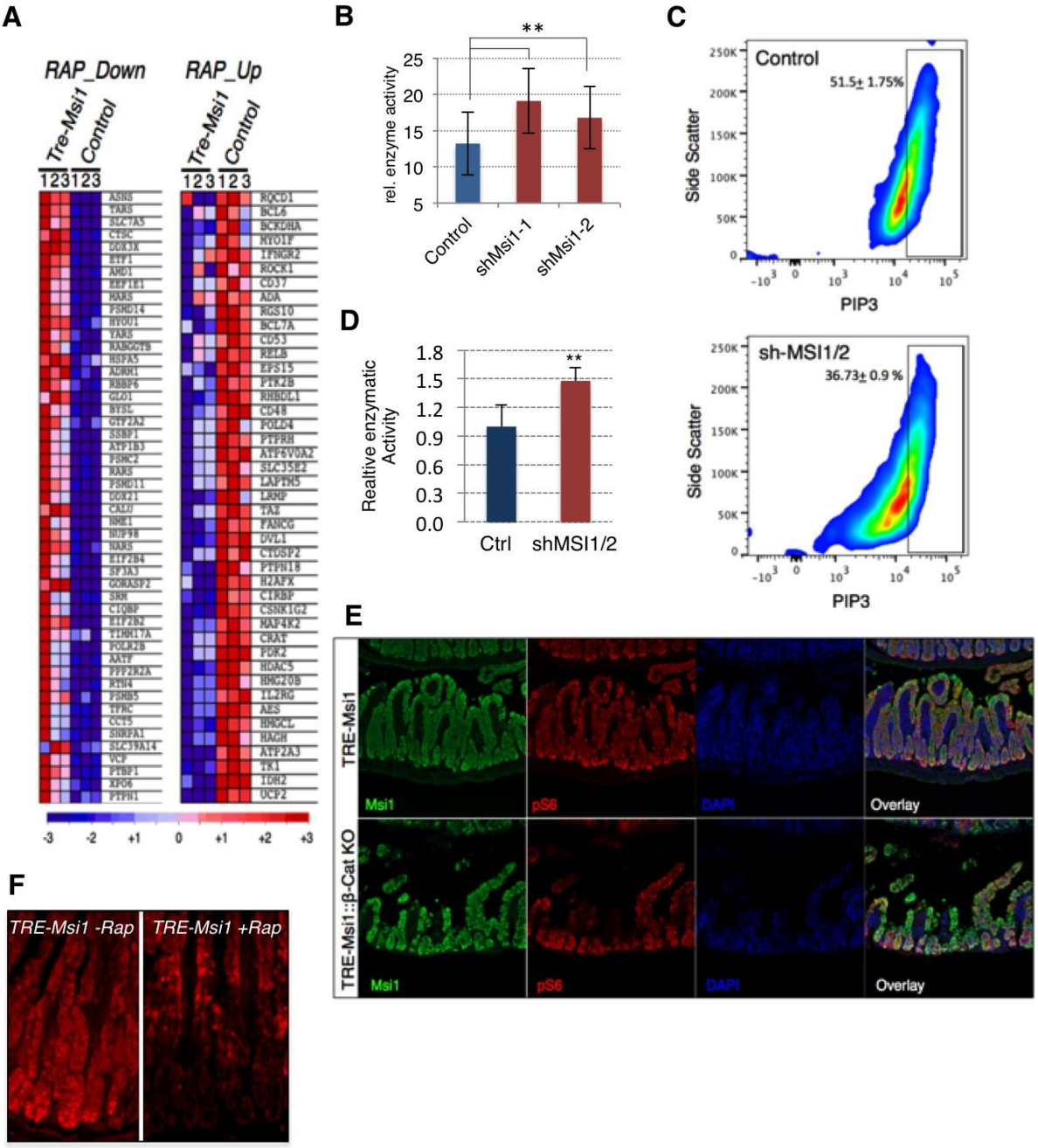

Figure S5. A. Heatmap showing upregulation of genes suppressed by Rapamycin treatment in *TRE-Msi1* epithelium (left) and a suppression of genes induced by Rapamycin treatment (right). **B.** PTEN enzymatic activity (measured by immunoprecipitation followed by ELISA) increases upon knockdown of MSI1 in 293T cells (**: $p < 0.005$). **C.** Representative flow cytometric analysis of PIP3 in LoVo cells upon knockdown of MSI1 and MSI2. **D**. PTEN enzymatic activity (measured by immunoprecipitation followed by ELISA) increases upon knockdown of MSI1/2 in RKO cells versus scrambled shRNA control (**: $p < 0.005$). **E.** Immunofluorescence staining for Msi1 and phospho-S6 in *TRE-Msi1* mice (top) and *TRE-Msi1:: Ctnnb1*$^{flox/flox}$*::VillinCreERT2* (bottom). Note the induction of S6 phosphorylation despite the loss of structural integrity of the epithelium upon ablation of β-catenin (100x). **F.** *TRE-Msi1* mice treated with Rapamycin 3 days prior to Dox induction of Msi1 for 48 hours stained for S6 phosphorylation by the mTORC1 target S6 kinase (mag. 200x). Refers to main **Figure 6.**

Supplemental Figure 6

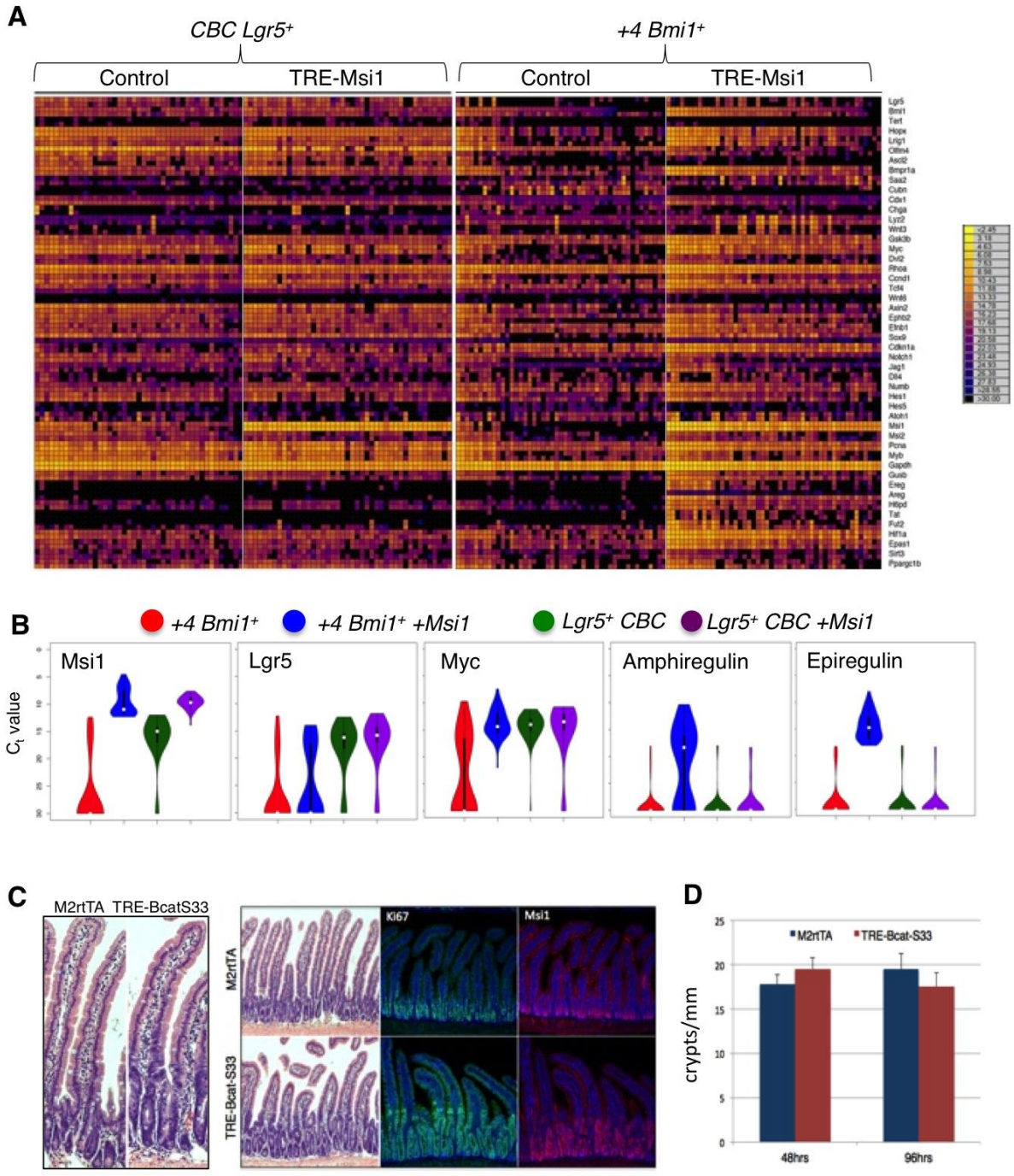

Figure S6. A. Heatmap showing Fluidigm Biomark profiling of Lgr5$^+$ and Bmi1$^+$ ISCs, both in the absence (control) and presence of Msi1 induction. Every column contains a single cell, and every row a single primer pair, with two distinct primer sets being used to interrogate each of the transcripts listed on the right. Colors correspond directly to Ct value, black being >30 (no detectable transcript). **B.** Violin plots showing the expression level in the populations of single cells in (**A**). The white dot in the violin plot represents the median expression within the group of cells, the black box represents the interquartile range. **C.** Effects of ectopic expression of constitutively active β-catenin in the small intestine reveal an expanded crypt proliferative zone marked by Ki67 (green) and Msi1 (red), without gross defects in differentiation along the crypt-villus axis (mag. 100x). **D.** Induction of constitutively active β-catenin reveals no significant change in crypt fission after 48 or 96 hours of Dox treatment. Refers to main **Figure 7.**

Presentation of results:

Data generated during this award have been presented at various scientific symposia. Students and Postdoctoral fellows have presented portions of this work at:

The annual retreat of the NIH P30 Center for Molecular Studies in Liver and Digestive Diseases, as well as internal meetings of the University of Pennsylvania Institute for Regenerative Medicine, Cell and Molecular Biology Graduate Program Research Retreat, Department of Animal Biology Seminar Series, the Development and Stem Cell Biology Graduate Subprogram Chalk Talk series, and our internal weekly lab meetings.

In addition, the Principle Investigator, Dr. Lengner, has presented this work at numerous venues, including as an invited speaker at the following:

The Mayo Clinic, Rochester MN
The Annual Meeting of the International Society for Stem Cell Research (Vancouver, BC)
The Mid-Atlantic Society for Developmental Biology Annual Meeting (Johns Hopkins)
The China Agricultural University, Beijing, China
The University of Massachusetts Medical School

References

Barker, N., Ridgway, R.A., van Es, J.H., van de Wetering, M., Begthel, H., van den Born, M., Danenberg, E., Clarke, A.R., Sansom, O.J., and Clevers, H. (2009). Crypt stem cells as the cells-of-origin of intestinal cancer. Nature *457*, 608-611.
Barker, N., van Es, J.H., Kuipers, J., Kujala, P., van den Born, M., Cozijnsen, M., Haegebarth, A., Korving, J., Begthel, H., Peters, P.J., *et al.* (2007). Identification of stem cells in small intestine and colon by marker gene Lgr5. Nature *449*, 1003-1007.
Battelli, C., Nikopoulos, G.N., Mitchell, J.G., and Verdi, J.M. (2006). The RNA-binding protein Musashi-1 regulates neural development through the translational repression of p21WAF-1. Mol Cell Neurosci *31*, 85-96.
Beard, C., Hochedlinger, K., Plath, K., Wutz, A., and Jaenisch, R. (2006). Efficient method to generate single-copy transgenic mice by site-specific integration in embryonic stem cells.

Genesis *44*, 23-28.
Chi, S.W., Zang, J.B., Mele, A., and Darnell, R.B. (2009). Argonaute HITS-CLIP decodes microRNA-mRNA interaction maps. Nature *460*, 479-486.
de Lau, W., Barker, N., Low, T.Y., Koo, B.K., Li, V.S., Teunissen, H., Kujala, P., Haegebarth, A., Peters, P.J., van de Wetering, M., *et al.* (2011). Lgr5 homologues associate with Wnt receptors and mediate R-spondin signalling. Nature *476*, 293-297.
Duvel, K., Yecies, J.L., Menon, S., Raman, P., Lipovsky, A.I., Souza, A.L., Triantafellow, E., Ma, Q., Gorski, R., Cleaver, S., *et al.* (2010). Activation of a metabolic gene regulatory network downstream of mTOR complex 1. Molecular cell *39*, 171-183.
el Marjou, F., Janssen, K.P., Chang, B.H., Li, M., Hindie, V., Chan, L., Louvard, D., Chambon, P., Metzger, D., and Robine, S. (2004). Tissue-specific and inducible Cre-mediated recombination in the gut epithelium. Genesis *39*, 186-193.
Fevr, T., Robine, S., Louvard, D., and Huelsken, J. (2007). Wnt/beta-catenin is essential for intestinal homeostasis and maintenance of intestinal stem cells. Mol Cell Biol *27*, 7551-7559.
Fre, S., Huyghe, M., Mourikis, P., Robine, S., Louvard, D., and Artavanis-Tsakonas, S. (2005). Notch signals control the fate of immature progenitor cells in the intestine. Nature *435*, 964-968.
Fujishita, T., Aoki, K., Lane, H.A., Aoki, M., and Taketo, M.M. (2008). Inhibition of the mTORC1 pathway suppresses intestinal polyp formation and reduces mortality in ApcDelta716 mice. Proceedings of the National Academy of Sciences of the United States of America *105*, 13544-13549.
Garcia, J.M., Rodriguez, R., Silva, J., Munoz, C., Dominguez, G., Silva, J.M., Carcereny, E., Provencio, M., Espana, P., and Bonilla, F. (2003). Intratumoral heterogeneity in microsatellite alterations in BRCA1 and PTEN regions in sporadic colorectal cancer. Ann Surg Oncol *10*, 876-881.
Goel, A., Arnold, C.N., Niedzwiecki, D., Carethers, J.M., Dowell, J.M., Wasserman, L., Compton, C., Mayer, R.J., Bertagnolli, M.M., and Boland, C.R. (2004). Frequent inactivation of PTEN by promoter hypermethylation in microsatellite instability-high sporadic colorectal cancers. Cancer research *64*, 3014-3021.
He, X.C., Yin, T., Grindley, J.C., Tian, Q., Sato, T., Tao, W.A., Dirisina, R., Porter-Westpfahl, K.S., Hembree, M., Johnson, T., *et al.* (2007). PTEN-deficient intestinal stem cells initiate intestinal polyposis. Nat Genet *39*, 189-198.
Hirata, A., Utikal, J., Yamashita, S., Aoki, H., Watanabe, A., Yamamoto, T., Okano, H., Bardeesy, N., Kunisada, T., Ushijima, T., *et al.* (2013). Dose-dependent roles for canonical Wnt signalling in de novo crypt formation and cell cycle properties of the colonic epithelium. Development *140*, 66-75.
Hope, K.J., Cellot, S., Ting, S.B., MacRae, T., Mayotte, N., Iscove, N.N., and Sauvageau, G. (2010). An RNAi screen identifies Msi2 and Prox1 as having opposite roles in the regulation of hematopoietic stem cell activity. Cell Stem Cell *7*, 101-113.
Imai, T., Tokunaga, A., Yoshida, T., Hashimoto, M., Mikoshiba, K., Weinmaster, G., Nakafuku, M., and Okano, H. (2001). The neural RNA-binding protein Musashi1 translationally regulates mammalian numb gene expression by interacting with its mRNA. Mol Cell Biol *21*, 3888-3900.
Ireland, H., Houghton, C., Howard, L., and Winton, D.J. (2005). Cellular inheritance of a Cre-activated reporter gene to determine Paneth cell longevity in the murine small intestine. Developmental dynamics : an official publication of the American Association of Anatomists *233*, 1332-1336.
Ito, T., Kwon, H.Y., Zimdahl, B., Congdon, K.L., Blum, J., Lento, W.E., Zhao, C., Lagoo, A.,

Gerrard, G., Foroni, L., *et al.* (2010). Regulation of myeloid leukaemia by the cell-fate determinant Musashi. Nature *466*, 765-768.
Itzkovitz, S., Lyubimova, A., Blat, I.C., Maynard, M., van Es, J., Lees, J., Jacks, T., Clevers, H., and van Oudenaarden, A. (2012). Single-molecule transcript counting of stem-cell markers in the mouse intestine. Nature cell biology *14*, 106-114.
Kawahara, H., Imai, T., Imataka, H., Tsujimoto, M., Matsumoto, K., and Okano, H. (2008). Neural RNA-binding protein Musashi1 inhibits translation initiation by competing with eIF4G for PABP. J Cell Biol *181*, 639-653.
Kharas, M.G., Lengner, C.J., Al-Shahrour, F., Bullinger, L., Ball, B., Zaidi, S., Morgan, K., Tam, W., Paktinat, M., Okabe, R., *et al.* Musashi-2 regulates normal hematopoiesis and promotes aggressive myeloid leukemia. Nat Med *16*, 903-908.
Kharas, M.G., Lengner, C.J., Al-Shahrour, F., Bullinger, L., Ball, B., Zaidi, S., Morgan, K., Tam, W., Paktinat, M., Okabe, R., *et al.* (2010). Musashi-2 regulates normal hematopoiesis and promotes aggressive myeloid leukemia. Nat Med *16*, 903-908.
Kinzler, K.W., Nilbert, M.C., Su, L.K., Vogelstein, B., Bryan, T.M., Levy, D.B., Smith, K.J., Preisinger, A.C., Hedge, P., McKechnie, D., *et al.* (1991). Identification of FAP locus genes from chromosome 5q21. Science *253*, 661-665.
Koehl, G.E., Spitzner, M., Ousingsawat, J., Schreiber, R., Geissler, E.K., and Kunzelmann, K. (2010). Rapamycin inhibits oncogenic intestinal ion channels and neoplasia in APC(Min/+) mice. Oncogene *29*, 1553-1560.
Koziczak, M., and Hynes, N.E. (2004). Cooperation between fibroblast growth factor receptor-4 and ErbB2 in regulation of cyclin D1 translation. The Journal of biological chemistry *279*, 50004-50011.
Langmead, B., Trapnell, C., Pop, M., and Salzberg, S.L. (2009). Ultrafast and memory-efficient alignment of short DNA sequences to the human genome. Genome Biol *10*, R25.
Levin, T.G., Powell, A.E., Davies, P.S., Silk, A.D., Dismuke, A.D., Anderson, E.C., Swain, J.R., and Wong, M.H. (2010). Characterization of the intestinal cancer stem cell marker CD166 in the human and mouse gastrointestinal tract. Gastroenterology *139*, 2072-2082 e2075.
Li, D., Peng, X., Yan, D., Tang, H., Huang, F., Yang, Y., and Peng, Z. (2011). Msi-1 is a predictor of survival and a novel therapeutic target in colon cancer. Ann Surg Oncol *18*, 2074-2083.
Liu, C., Li, Y., Semenov, M., Han, C., Baeg, G.H., Tan, Y., Zhang, Z., Lin, X., and He, X. (2002). Control of beta-catenin phosphorylation/degradation by a dual-kinase mechanism. Cell *108*, 837-847.
Maria Cambuli, F., Rezza, A., Nadjar, J., and Plateroti, M. (2013). Brief report: musashi1-eGFP mice, a new tool for differential isolation of the intestinal stem cell populations. Stem cells *31*, 2273-2278.
Merlos-Suarez, A., Barriga, F.M., Jung, P., Iglesias, M., Cespedes, M.V., Rossell, D., Sevillano, M., Hernando-Momblona, X., da Silva-Diz, V., Munoz, P., *et al.* The intestinal stem cell signature identifies colorectal cancer stem cells and predicts disease relapse. Cell Stem Cell *8*, 511-524.
Merlos-Suarez, A., Barriga, F.M., Jung, P., Iglesias, M., Cespedes, M.V., Rossell, D., Sevillano, M., Hernando-Momblona, X., da Silva-Diz, V., Munoz, P., *et al.* (2011). The intestinal stem cell signature identifies colorectal cancer stem cells and predicts disease relapse. Cell stem cell *8*, 511-524.
Miyoshi, Y., Nagase, H., Ando, H., Horii, A., Ichii, S., Nakatsuru, S., Aoki, T., Miki, Y., Mori,

T., and Nakamura, Y. (1992). Somatic mutations of the APC gene in colorectal tumors: mutation cluster region in the APC gene. Hum Mol Genet *1*, 229-233.
Montgomery, R.K., Carlone, D.L., Richmond, C.A., Farilla, L., Kranendonk, M.E., Henderson, D.E., Baffour-Awuah, N.Y., Ambruzs, D.M., Fogli, L.K., Algra, S., *et al.* Mouse telomerase reverse transcriptase (mTert) expression marks slowly cycling intestinal stem cells. Proc Natl Acad Sci U S A *108*, 179-184.
Munoz, J., Stange, D.E., Schepers, A.G., van de Wetering, M., Koo, B.K., Itzkovitz, S., Volckmann, R., Kung, K.S., Koster, J., Radulescu, S., *et al.* (2012). The Lgr5 intestinal stem cell signature: robust expression of proposed quiescent '+4' cell markers. The EMBO journal *31*, 3079-3091.
Nagase, H., Miyoshi, Y., Horii, A., Aoki, T., Petersen, G.M., Vogelstein, B., Maher, E., Ogawa, M., Maruyama, M., Utsunomiya, J., *et al.* (1992). Screening for germ-line mutations in familial adenomatous polyposis patients: 61 new patients and a summary of 150 unrelated patients. Hum Mutat *1*, 467-473.
Nakamura, M., Okano, H., Blendy, J.A., and Montell, C. (1994). Musashi, a neural RNA-binding protein required for Drosophila adult external sensory organ development. Neuron *13*, 67-81.
Park, S.M., Deering, R.P., Lu, Y., Tivnan, P., Lianoglou, S., Al-Shahrour, F., Ebert, B.L., Hacohen, N., Leslie, C., Daley, G.Q., *et al.* (2014). Musashi-2 controls cell fate, lineage bias, and TGF-beta signaling in HSCs. J Exp Med *211*, 71-87.
Potten, C.S., Booth, C., Tudor, G.L., Booth, D., Brady, G., Hurley, P., Ashton, G., Clarke, R., Sakakibara, S., and Okano, H. (2003). Identification of a putative intestinal stem cell and early lineage marker; musashi-1. Differentiation; research in biological diversity *71*, 28-41.
Powell, A.E., Wang, Y., Li, Y., Poulin, E.J., Means, A.L., Washington, M.K., Higginbotham, J.N., Juchheim, A., Prasad, N., Levy, S.E., *et al.* (2012). The pan-ErbB negative regulator Lrig1 is an intestinal stem cell marker that functions as a tumor suppressor. Cell *149*, 146-158.
Ramalho-Santos, M., Yoon, S., Matsuzaki, Y., Mulligan, R.C., and Melton, D.A. (2002). "Stemness": transcriptional profiling of embryonic and adult stem cells. Science *298*, 597-600.
Rezza, A., Skah, S., Roche, C., Nadjar, J., Samarut, J., and Plateroti, M. (2010). The overexpression of the putative gut stem cell marker Musashi-1 induces tumorigenesis through Wnt and Notch activation. J Cell Sci *123*, 3256-3265.
Rhodes, D.R., Kalyana-Sundaram, S., Mahavisno, V., Varambally, R., Yu, J., Briggs, B.B., Barrette, T.R., Anstet, M.J., Kincead-Beal, C., Kulkarni, P., *et al.* (2007). Oncomine 3.0: genes, pathways, and networks in a collection of 18,000 cancer gene expression profiles. Neoplasia *9*, 166-180.
Sakakibara, S., Nakamura, Y., Yoshida, T., Shibata, S., Koike, M., Takano, H., Ueda, S., Uchiyama, Y., Noda, T., and Okano, H. (2002). RNA-binding protein Musashi family: roles for CNS stem cells and a subpopulation of ependymal cells revealed by targeted disruption and antisense ablation. Proceedings of the National Academy of Sciences of the United States of America *99*, 15194-15199.
Sangiorgi, E., and Capecchi, M.R. (2008). Bmi1 is expressed in vivo in intestinal stem cells. Nature genetics *40*, 915-920.
Sansom, O.J., Reed, K.R., Hayes, A.J., Ireland, H., Brinkmann, H., Newton, I.P., Batlle, E., Simon-Assmann, P., Clevers, H., Nathke, I.S., *et al.* (2004). Loss of Apc in vivo immediately perturbs Wnt signaling, differentiation, and migration. Genes & development *18*, 1385-1390.
Sato, T., Vries, R.G., Snippert, H.J., van de Wetering, M., Barker, N., Stange, D.E., van Es, J.H., Abo, A., Kujala, P., Peters, P.J., *et al.* (2009). Single Lgr5 stem cells build crypt-villus structures

in vitro without a mesenchymal niche. Nature *459*, 262-265.
Spears, E., and Neufeld, K.L. (2011). Novel double-negative feedback loop between adenomatous polyposis coli and Musashi1 in colon epithelia. J Biol Chem *286*, 4946-4950.
Stanger, B.Z., Datar, R., Murtaugh, L.C., and Melton, D.A. (2005). Direct regulation of intestinal fate by Notch. Proc Natl Acad Sci U S A *102*, 12443-12448.
Subramanian, A., Tamayo, P., Mootha, V.K., Mukherjee, S., Ebert, B.L., Gillette, M.A., Paulovich, A., Pomeroy, S.L., Golub, T.R., Lander, E.S., *et al.* (2005). Gene set enrichment analysis: a knowledge-based approach for interpreting genome-wide expression profiles. Proceedings of the National Academy of Sciences of the United States of America *102*, 15545-15550.
Sureban, S.M., May, R., George, R.J., Dieckgraefe, B.K., McLeod, H.L., Ramalingam, S., Bishnupuri, K.S., Natarajan, G., Anant, S., and Houchen, C.W. (2008). Knockdown of RNA binding protein musashi-1 leads to tumor regression in vivo. Gastroenterology *134*, 1448-1458.
Takeda, N., Jain, R., LeBoeuf, M.R., Wang, Q., Lu, M.M., and Epstein, J.A. Interconversion between intestinal stem cell populations in distinct niches. Science *334*, 1420-1424.
Takeda, N., Jain, R., LeBoeuf, M.R., Wang, Q., Lu, M.M., and Epstein, J.A. (2011). Interconversion between intestinal stem cell populations in distinct niches. Science *334*, 1420-1424.
Tian, H., Biehs, B., Warming, S., Leong, K.G., Rangell, L., Klein, O.D., and de Sauvage, F.J. (2011). A reserve stem cell population in small intestine renders Lgr5-positive cells dispensable. Nature *478*, 255-259.
Ule, J., Jensen, K.B., Ruggiu, M., Mele, A., Ule, A., and Darnell, R.B. (2003). CLIP identifies Nova-regulated RNA networks in the brain. Science *302*, 1212-1215.
van de Wetering, M., Sancho, E., Verweij, C., de Lau, W., Oving, I., Hurlstone, A., van der Horn, K., Batlle, E., Coudreuse, D., Haramis, A.P., *et al.* (2002). The beta-catenin/TCF-4 complex imposes a crypt progenitor phenotype on colorectal cancer cells. Cell *111*, 241-250.
Wang, T., Ong, C.W., Shi, J., Srivastava, S., Yan, B., Cheng, C.L., Yong, W.P., Chan, S.L., Yeoh, K.G., Iacopetta, B., *et al.* (2011). Sequential expression of putative stem cell markers in gastric carcinogenesis. British journal of cancer *105*, 658-665.
Wasan, H.S., Park, H.S., Liu, K.C., Mandir, N.K., Winnett, A., Sasieni, P., Bodmer, W.F., Goodlad, R.A., and Wright, N.A. (1998). APC in the regulation of intestinal crypt fission. J Pathol *185*, 246-255.
Yan, K.S., Chia, L.A., Li, X., Ootani, A., Su, J., Lee, J.Y., Su, N., Luo, Y., Heilshorn, S.C., Amieva, M.R., *et al.* (2012). The intestinal stem cell markers Bmi1 and Lgr5 identify two functionally distinct populations. Proceedings of the National Academy of Sciences of the United States of America *109*, 466-471.
Zhou, X., Tan, M., Stone Hawthorne, V., Klos, K.S., Lan, K.H., Yang, Y., Yang, W., Smith, T.L., Shi, D., and Yu, D. (2004). Activation of the Akt/mammalian target of rapamycin/4E-BP1 pathway by ErbB2 overexpression predicts tumor progression in breast cancers. Clinical cancer research : an official journal of the American Association for Cancer Research *10*, 6779-6788.

18. Extent of Clinical Activities Initiated and Completed. Items 18(A) and 18(B) should be completed for all research projects. If the project was restricted to secondary analysis of clinical data or data analysis of clinical research, then responses to 18(A) and 18(B) should be "No."

18(A) Did you initiate a study that involved the testing of treatment, prevention or diagnostic procedures on human subjects?

_____Yes
____X_No

18(B) Did you complete a study that involved the testing of treatment, prevention or diagnostic procedures on human subjects?

_____Yes
___X__No

If "Yes" to either 18(A) or 18(B), items 18(C) – (F) must also be completed. (Do NOT complete 18(C-F) if 18(A) and 18(B) are both "No.")

18(C) How many hospital and health care professionals were involved in the research project?

_____Number of hospital and health care professionals involved in the research project

18(D) How many subjects were included in the study compared to targeted goals?

_____Number of subjects originally targeted to be included in the study
_____Number of subjects enrolled in the study

Note: Studies that fall dramatically short on recruitment are encouraged to provide the details of their recruitment efforts in Item 17, Progress in Achieving Research Goals, Objectives and Aims. For example, the number of eligible subjects approached, the number that refused to participate and the reasons for refusal. Without this information it is difficult to discern whether eligibility criteria were too restrictive or the study simply did not appeal to subjects.

18(E) How many subjects were enrolled in the study by gender, ethnicity and race?

Gender:
_____Males
_____Females
_____Unknown

Ethnicity:
_____Latinos or Hispanics
_____Not Latinos or Hispanics
_____Unknown

Race:
_____American Indian or Alaska Native
_____Asian
_____Blacks or African American
_____Native Hawaiian or Other Pacific Islander
_____White
_____Other, specify:_____
_____Unknown

18(F) Where was the research study conducted? (List the county where the research study was conducted. If the treatment, prevention and diagnostic tests were offered in more than one county, list all of the counties where the research study was conducted.)

19. Human Embryonic Stem Cell Research. Item 19(A) should be completed for all research projects. If the research project involved human embryonic stem cells, items 19(B) and 19(C) must also be completed.

19(A) Did this project involve, in any capacity, human embryonic stem cells?
_____Yes
___X__No

19(B) Were these stem cell lines NIH-approved lines that were derived outside of Pennsylvania?
_____Yes
_____ No

19(C) Please describe how this project involved human embryonic stem cells:

20. Articles Submitted to Peer-Reviewed Publications.

20(A) Identify all publications that resulted from the research performed during the funding period and that have been submitted to peer-reviewed publications. Do not list journal abstracts or presentations at professional meetings; abstract and meeting presentations should be listed at the end of item 17. **Include only those publications that acknowledge the Pennsylvania Department of Health as a funding source** (as required in the grant agreement). List the title of the journal article, the authors, the name of the peer-reviewed publication, the month and year when it was submitted, and the status of publication (submitted for publication, accepted for publication or published.). Submit an electronic copy of each publication or paper submitted for publication, listed in the table, in a PDF version 5.0.5 (or greater) format, 1,200 dpi. Filenames for each publication should include the number of the research project, the last name of the PI, and an abbreviated title of the publication. For example, if you submit two publications for Smith (PI for Project 01), one

publication for Zhang (PI for Project 03), and one publication for Bates (PI for Project 04), the filenames would be:

Project 01 – Smith – Three cases of isolated
Project 01 – Smith – Investigation of NEB1 deletions
Project 03 – Zhang – Molecular profiling of aromatase
Project 04 – Bates – Neonatal intensive care

If the publication is not available electronically, provide 5 paper copies of the publication.

Note: The grant agreement requires that recipients acknowledge the Pennsylvania Department of Health funding in all publications. Please ensure that all publications listed acknowledge the Department of Health funding. If a publication does not acknowledge the funding from the Commonwealth, do not list the publication.

Title of Journal Article:	Authors:	Name of Peer-reviewed Publication:	Month and Year Submitted:	Publication Status (check appropriate box below):
1. Transformation of the intestinal epithelium by the MSI2 RNA binding protein	Shan Wang, Ning Li, Maryam Yousefi, Angela Nakauka-Ddamba, Fan Li, Kimberly Parada, Shilpa Rao, Gerard Minuesa, Yarden Katz, Brian D. Gregory, Michael G. Kharas, Zhengquan Yu, and Christopher J. Lengner	Nature Communications	December 2014	☐Submitted ☒ Accepted ☐Published

20(B) Based on this project, are you planning to submit articles to peer-reviewed publications in the future?

Yes___X____ No_____

If yes, please describe your plans:

We are currently preparing a manuscript describing the role of Msi proteins in governing dormant stem cell activation during normal intestinal homeostasis and during regeneration after tissue injury. We anticipate this manuscript will be submitted before the first of April 2015. After that we are in the early stages of follow-up work studying the importance of these dormant stem cells to tumor maintenance in mouse models.

21. Changes in Outcome, Impact and Effectiveness Attributable to the Research Project. Describe the outcome, impact, and effectiveness of the research project by summarizing its impact on the incidence of disease, death from disease, stage of disease at time of diagnosis, or other relevant measures of outcome, impact or effectiveness of the research project. If

there were no changes, insert "None"; do not use "Not applicable." Responses must be single-spaced below, and no smaller than 12-point type. DO NOT DELETE THESE INSTRUCTIONS. There is no limit to the length of your response.

None.

22. Major Discoveries, New Drugs, and New Approaches for Prevention Diagnosis and Treatment. Describe major discoveries, new drugs, and new approaches for prevention, diagnosis and treatment that are attributable to the completed research project. If there were no major discoveries, drugs or approaches, insert "None"; do not use "Not applicable." Responses must be single-spaced below, and no smaller than 12-point type. DO NOT DELETE THESE INSTRUCTIONS. There is no limit to the length of your response.

The discoveries of this project are twofold. First, our findings demonstrate that Msi proteins are a valid therapeutic target for small molecule inhibition to reactivate tumor suppressors in colorectal cancers. Collaborating laboratories are currently conducting high content small molecule screens to identify Msi inhibitors. Secondly, and more importantly, our findings shift the dogma of how colorectal cancer initiation and maintenance is viewed. For the past decade or so, it was believed that the 'active' intestinal stem cell with high Wnt pathway activity was the critical cancer stem cell. Our findings open a new door for investigating the potential contribution of a second, dormant stem cell that sits at the top of the intestinal stem cell hierarchy and gives rise to active intestinal stem cells, as a major driver of colon cancer. We know that these dormant stem cells, unlike their active counterparts, are highly resistant to damage such as high-dose gamma irradiation. Thus, we are highly interested in investigating whether it is the counterpart of these cells that represent the chemo- and radio-resistant cancer stem cell possibly responsible for tumor recurrence after surgical resection and traditional therapeutic interventions. We believe that our findings will lead to a host of new investigations into novel therapeutic modalities specifically targeting these dormant stem cells, which, to date, have yet to be directly observed in human tissue.

23. Inventions, Patents and Commercial Development Opportunities.

23(A) Were any inventions, which may be patentable or otherwise protectable under Title 35 of the United States Code, conceived or first actually reduced to practice in the performance of work under this health research grant? Yes_____ No____X

If "Yes" to 23(A), complete items a – g below for each invention. (Do NOT complete items a - g if 23(A) is "No.")

a. Title of Invention:

b. Name of Inventor(s):

c. Technical Description of Invention (describe nature, purpose, operation and physical, chemical, biological or electrical characteristics of the invention):

d. Was a patent filed for the invention conceived or first actually reduced to practice in the performance of work under this health research grant?
Yes_____ No___

If yes, indicate date patent was filed:

e. Was a patent issued for the invention conceived or first actually reduced to practice in the performance of work under this health research grant?
Yes_____ No___
If yes, indicate number of patent, title and date issued:
Patent number:
Title of patent:
Date issued:

f. Were any licenses granted for the patent obtained as a result of work performed under this health research grant? Yes_____ No___

If yes, how many licenses were granted?_____

g. Were any commercial development activities taken to develop the invention into a commercial product or service for manufacture or sale? Yes__ No___

If yes, describe the commercial development activities:

23(B) Based on the results of this project, are you planning to file for any licenses or patents, or undertake any commercial development opportunities in the future?

Yes_____ No_____X__

If yes, please describe your plans:

24. Key Investigator Qualifications. Briefly describe the education, research interests and experience and professional commitments of the Principal Investigator and all other key investigators. In place of narrative you may insert the NIH biosketch form here; however, please limit each biosketch to 1-2 pages.

Christopher Lengner, PhD

INSTITUTION AND LOCATION	DEGREE	YEARS	FIELD OF STUDY
Worcester Polytechnic Institute, Worcester, MA	B.S.	1994-1998	Biotechnology
Univ. of Massachusetts Medical School, Worcester, MA	Ph.D.	1998-2004	Cell and Molecular Biology
Whitehead Institute for Biomedical Research (MIT), Cambridge, MA	Post Doc	2005-2010	Stem Cell Genetics

Personal Statement

The overarching goal of my research program is to gain an understanding of the molecular mechanisms that govern stem cell potency and how dysregulation of these mechanisms can contribute to disease onset and progression, such as oncogenesis. We employ genetic, genomic, and single-cell analysis approaches in murine systems to address these fundamental questions, and, in parallel, utilize human pluripotent cell-derived culture systems to translate findings into patient-derived models. Using these approaches we have identified novel tumorigenic pathways underlying the ontogeny of hematopoietic and gastrointestinal cancers which are subsequently being assessed as potential points for therapuetic intervention. We have also begun to unravel the heirarchical structure of the intestinal stem cell compartment with the ultimate goal of understanding how perturbations in this hierarchy contribute to disease states.

Positions and Honors

1997-1998 Undergraduate Research Assistant, Worcester Polytechnic Institute, Department of Cell Biology, University of Massachusetts Medical School, Jane B. Lian Laboratory
1998-2005 Graduate Research Assistant, University of Massachusetts Medical School, Department of Cell Biology, Gary S. Stein Laboratory
2001-2005 Member, American Society for Bone and Mineral Research
2004 American Society for Bone and Mineral Research Young Investigator Award
2005-2010 Postdoctoral Fellow, Whitehead Institute for Biomedical Research, Rudolf Jaenisch Laboratory
2006-2009 NIH Ruth L. Kirschstein NRSA Fellow
2006-Present Member, International Society for Stem Cell Research
2011-Present Assistant Professor, Department of Animal Biology, School of Veterinary Medicine and Institute for Regenerative Medicine, Center for Liver and Digestive Diseases, and Department of Cell & Developmental Biology, School of Medicine, University of Pennsylvania
2012 W.W. Smith Charitable Trust Cancer Scholar

Select peer-reviewed Publications

1. Lengner CJ*, Steinman HA*, Gagnon J, Smith TW, Henderson JE, Kream BE, Stein GS, Lian JB, Jones SN. (2006) Osteoblast differentiation and skeletal development are

regulated by Mdm2-p53 signaling. ***Journal of Cell Biology***. 2006 Mar 13; 172(6): 909-21. **Authors contributed equally* PMID: 16533949 PMCID: PMC2063734

2. Lengner CJ, Camargo FD, Hochedlinger K, Welstead GG, Zaidi S Gokhale S, Scholer HR, Tomilin A, and Jaenisch R. (2007) Oct4 expression is not required for mouse somatic stem cell self-renewal. ***Cell Stem Cell*** Oct; 1(4). PMID: 18159219 PMCID: PMC2151746
3. Brambrink T*, Foreman R*, Welstead GG*, Lengner CJ, Wernig M, Suh H, and Jaenisch R. (2008) Sequential expression of pluripotency markers and downregulation of transgenes during direct reprogramming of somatic cells. ***Cell Stem Cell*** Feb; 2(2). **Authors contributed equally* PMID: 18371436 PMCID: PMC2276627
4. Hanna J, Markoulaki S, Schorderet P, Carey BW, Beard C, Wernig M, Creyghton MP, Steine EJ, Cassady JP, Foreman R, Lengner CJ, Dausman JA, Jaenisch R. (2008) Direct reprogramming of terminally differentiated mature B lymphocytes to pluripotency. ***Cell*** Apr 18;133(2):250-64. PMID: 18423197 PMCID: PMC2615249
5. Wernig M*, Lengner CJ*, Hanna J, Lodato MA, Steine E, Foreman R, Staerk J, Markoulaki S, and Jaenisch R. (2008) A drug-inducible transgenic system for direct reprogramming of multiple somatic cell types. ***Nature Biotechnology*** Aug;26(8):916-24**.** **Authors contributed equally* PMID: 18594521 PMCID: PMC2654269
6. Markoulaki S*, Hanna J*, Beard C, Carey BW, Cheng AW, Lengner CJ, Dausman JA, Fu D, Gao Q, Wu S, Cassady JP, Jaenisch R. (2009) Transgenic mice with defined combinations of drug-inducible reprogramming factors. ***Nature Biotechnology*** Feb;27(2):169-71*Authors contributed equally PMID: 19151700 PMCID: PMC2654270
7. Hanna J*, Markoulaki S*, Mitalipova M, Cheng AW, Cassady JP, Staerk J, Carey BW, Lengner CJ**,** Foreman R, Love J, Gao Q, Kim J, Jaenisch R. (2009) Metastable Pluripotent States in NOD-Mouse-Derived ESCs. ***Cell Stem Cell*** Jun 5;4(6):513-524. *Authors contributed equally PMID: 19427283 PMCID: PMC2714944
8. Hanna J*, Saha K*, Pando B, van Zon J, Lengner CJ, Creyghton MP, van Oudenaarden A, and Jaenisch R. (2009) Direct reprogramming is a stochastic process amenable to cell division rate dependent and independent acceleration. ***Nature*** Dec 3;462(7273):595-601. **Authors contributed equally* PMID: 19898493 PMCID: PMC2789972
9. Lengner CJ*, Gimelbrant AA*, Erwin JA, Cheng AW, Guenther MG, Welstead GG, Alagappan R, Frampton GM, Xu P, Muffat J, Santagata S, Powers D, Barrett CB, Young RA, Lee JT, Jaenisch R, Mitalipova M. (2010) Derivation of pre-X inactivation human embryonic stem cells under physiological oxygen concentrations. ***Cell*** May 28;141(5):872-83. **Authors contributed equally* PMID: 20471072
10. Kharas MG*, Lengner CJ*, Al-Shahrour F, Bullinger L, Ball B, Zaidi S, Morgan K, Tam W, Paktinat M, Okabe R, Gozo M, Scholl C, Frohling S, Fleming M, Ebert BL, Gilliland DG, Jaenisch R, and Daley GQ. (2010) Musashi-2 promotes hematopoietic stem cell proliferation and accelerates myeloid leukemogenesis. ***Nature Medicine*** Aug;16(8):903-8. **Authors contributed equally* PMID: 20616797 PMCID: PMC3090658
11. Kim J, Su SC, Wang H, Cheng AW, Cassady JP, Lodato MA, Lengner CJ, Chung CY, Dawlaty MM, Tsai LH, Jaenisch R. (2011) Functional Integration of Dopaminergic Neurons Directly Converted from Mouse Fibroblasts. ***Cell Stem Cell*** Oct 19. [Epub ahead of print]. PMID: 22019014 PCMID: PMC3210333
12. Park SM, Deering RP, Lu Y, Tivnan P, Lianoglou S, Al-Shahrour F, Ebert BL, Leslie C, Daley GQ, Lengner CJ, Kharas MG. Msi2 controls self-renewal, lineage restriction and

TGF-β signaling in HSCs. ***Journal of Experimental Medicine,*** 2014 Jan 13;211(1):71-87. doi: 10.1084/jem.20130736. Epub 2014 Jan 6. PMCID: PMC3892968

13. Yildirim O, Hung JH, Cedeno R, Weng Z, Lengner CJ***,** Rando OJ*****. "A system for genome-wide histone variant dynamics in ES cells reveals dynamic Macro-H2A replacement at promoters" ***PLoS Genetics,*** 2014 Aug 7;10(8):e1004515, 2014. PMCID: PMC4125097 *******Corresponding authors*

14. Li N, Yousefi M, Nakauka-Ddamba A, Jain R, Tobias J, Epstein JA, Jensen S, Lengner CJ. "Single cell analysis of proxy reporter allele-marked epithelial cells establishes intestinal stem cell hierarchy" ***Stem Cell Reports***, 2014 Nov 11;3(5):876-91. PMCID: PMC4235148

15. Wang N*, Li N*, Yousefi M, Nakauka-Ddamba A, Li F, Parada K, Rao S, Minuesa G, Katz Y, Gregory BD, Kharas MG, Yu Z, Lengner CJ. "Transformation of the intestinal epithelium by the MSI2 RNA binding protein" ***Nature Communications,*** 2014 In Press, PMCID in process. *******Authors contributed equally*

Research Support

Active

NIH R01CA168654-01 Lengner (PI)
Deregulation of MSI RNA-binding proteins promotes intestinal tumorigenesis
07/01/2012-06/30/2017

University of Pennsylvania Institute on Aging Lengner/Johnson (PIs)
Rescue of telomere dysfunction using genome editing and pharmacological approaches
07/01/2014-06/30/2015

Pending

R21AG051109(MPI)
Lengner/Johnson (PIs) A tractable model to address telomere dysfunction in a human tissue

R01DK106309
Lengner (PI) Control of gastrointestinal radiosensitivity by an Msi-mTorc1 signaling axis

R01OD019908(MPI)
Lengner/Brinster (PIs) Direct reprogramming of somatic cells into male germline stem cells